On the rootless nature of a Devonian suture in SW Iberia (Ossa-Morena Complex, Variscan Orogen): geometry and kinematics of the Azuaga Fault

Rubén Díez Fernández[1], Carlos Fernández[2], Ricardo Arenas[3], Irene Novo-Fernández[3]

[1]*Centro Nacional Instituto Geológico y Minero de España (CN-IGME), CSIC, Spain*

[2]*Departamento de Ciencias de la Tierra, Universidad de Huelva, Campus de El Carmen, 21071 Huelva, Spain (*)*

[3]*Departamento de Petrología y Geoquímica e Instituto de Geociencias (UCM, CSIC), Universidad Complutense, Madrid, Spain*

(*) Present address: Departamento de Geodinámica, Estratigrafía y Paleontología, Universidad Complutense, Madrid, Spain

Corresponding author: r.diez@igme.es

ABSTRACT

Suture zones are key to understand collisional orogens, but not all the remains of subduction leading to collision occur in the root of the suture. The Azuaga Fault bounds a Devonian suture zone known as Central Unit. This fault is a steeply NE-dipping, Variscan strike-slip fault with left-lateral and reverse oblique slip components formed during sinistral transpression in the Pennsylvanian. Motion along this fault was coeval with folding and fabric development in both its hanging wall and footwall and also with

This article has been accepted for publication and undergone full peer review but has not been through the copyediting, typesetting, pagination and proofreading process, which may lead to differences between this version and the Version of Record. Please cite this article as doi: 10.1029/2021TC006791.

the Matachel Fault. Tectonic flow associated with the Azuaga Fault shows high-vorticity, explaining the exhumation of a flat-lying Devonian suture zone via WNW-plunging extrusion from the upper-middle crust under inclined triclinic transpression during ENE-WSW convergence. The exposed basal contact of the Central Unit is not the root zone of a Variscan suture zone, but instead is a NE-dipping breaching fault that cuts across the suture zone that is contiguous to the SW under the upper section of the footwall. The peri-Gondwanan terrane between the Central Unit and the South-Portuguese Zone of the Iberian Massif (most of the Ossa-Morena Zone) is underlain by a Devonian suture, implying it is a continental allochthon. Variscan suture zones in Europe are affected by strike-slip faults. In our case, this pattern implies the location of suture zone exposures and location of its root are different. Suture zones and strike-slip faults are common in orogens and analysis of their relationships may lead to relocation of suture zone roots and re-thinking of upper and lower plates.

Keywords: Variscan Orogen; Suture Zone; SW Iberia; Ossa-Morena; Breaching fault

1. INTRODUCTION

Recognizing the major architecture of a collisional orogen relies on an understanding of its suture zone(s). The final structure and local geometry of a suture zone is typically the result of multiple deformation events, from the subduction that records convergence to the syn- and post-collisional structures responsible for the lithospheric thickening and/or thinning that follow (*Andersen et al.*, 1991; *Hatcher*, 1978; *Hodges*, 2000; *Matte*, 1986; *Platt*, 1986; *Vanderhaeghe*, 2012). The later structures influence the way a suture zone is exposed, and their recognition impacts on our understanding about how collisional orogens are built. Suture zones and strike-slip faults

are common in orogens worldwide (*Abdelsalam et al.*, 1998; *Dewey*, 1977; *Hirn et al.*, 1984; *Hutton*, 2009; *Oyhantçabal et al.*, 2011; *Taylor et al.*, 2003). In some cases, strike-slip faults can include oblique slip components and/or cut across the nappe structure of the orogen (*Brueckner et al.*, 2009; *Faure et al.*, 2009; *Guillot et al.*, 2009; *Martínez Catalán et al.*, 2020; *Pérez-Cáceres et al.*, 2015). Identification of the upper and lower plate to a suture zone that is affected by a strike-slip shear zone is heavily reliant on the (i) kinematics and (ii) tectonic flow associated with the motion along the shear zone as well as on the (iii) geometrical relationships between the suture and the shear zone (Figure 1).

The role of strike-slip faults in the final geometry of suture zones can be investigated in the Variscan Orogen (Fig. 2). Part of the internal architecture of this orogen is considered to derive from the suturing of more than one ocean basin (*Arenas et al.*, 2014; *Franke et al.*, 2017; *Shaw and Johnston*, 2016; *Simancas et al.*, 2005; *Wu et al.*, 2020), the rest of it resulting from the subsequent progressive collision between intervening landmasses, i.e. Laurussia, Gondwana, and other pericontinental terranes (*Díez Fernández et al.*, 2016; *Faure et al.*, 2009; *Kroner and Romer*, 2013; *Martínez Catalán et al.*, 2009; *Matte*, 1991; *Murphy et al.*, 2016). The number of ocean basins considered to be consumed varied from section to section along the orogen, resulting in models showing a complex pre- and syn-orogenic paleogeography (*Arenas et al.*, 2014; *Cocks and Torsvik*, 2002; *Franke*, 2000; *Franke et al.*, 2017; *Kroner and Romer*, 2013; *Simancas et al.*, 2005; *Stampfli et al.*, 2013). Models that incorporate a simpler pre-orogenic paleogeography with a lesser number of suture zones require that some long-standing ideas for the Variscan Orogen be disproved. Here we test the model that within the Iberian Massif there is a Devonian suture zone that is rooted along the boundary between the Ossa-Morena Domain to the south and the Obejo-Valsequillo Domain to the

north (*Azor et al.*, 1994) (Fig. 3). Contrary to this model, it has been proposed that the high-P metamorphic rocks exposed along this boundary represent a portion (not the root) of a Devonian suture zone that separates the Iberian Allochthon (ensemble containing far-traveled peri-Gondwanan terranes) from the Iberian Autochthon and Parautochthon (representing mainland Gondwana) (Fig. 3a; *Díez Fernández and Arenas*, 2015). The significance of identifying the rooted or rootless nature of the rocks defining this Devonian suture zone in SW Iberia is that the second (rootless) option implies the existence of a stack of allochthonous nappes of peri-Gondwanan terranes (Iberian Allochthon) that can be mapped along almost the entire orogenic hinterland (Fig. 3a). In addition it requires the existence of only two suture zones for the Variscan Orogen in Iberia; one separating peri-Gondwana terranes from Laurussia (suture of the Rheic Ocean *s.l.*), and another one separating those terranes from Gondwana (suture of a peri-Gondwana marginal basin).

Since oblique tectonics is the rule rather than the exception (e.g., Philippon and Corti, 2016), a detailed analysis of the kinematics of shear zones is a necessary condition for a correct understanding of orogenic belts. In particular, the study of late transpressional shear zones makes it possible to restore more rigorously the geometry of the structures associated with the previous stages, especially those due to the main phases of tectonic evolution of the orogenic belt. The Azuaga Fault zone was defined as a Variscan strike-slip structure that exposes a Devonian suture zone, referred to as the Central Unit, and separates Gondwanan terranes in SW Iberia (*Azor et al.*, 1994), i.e. the Ossa-Morena Domain from the Obejo-Valsequillo Domain (Fig. 3b). A detailed structural analysis of this fault zone and the blocks contained within it constrains the regional geometry and kinematics of this suture zone in the context of syn- to late-collisional activity associated with the Variscan Orogeny. Our analysis indicates that the NE-dipping

Azuaga Fault cuts across a more shallowly-dipping Devonian suture zone and transported it upwards in its hanging wall to its current exposure level. This interpretation implies that the Devonian suture zone continues SW-wards into the footwall rocks to the Azuaga Fault, underlying most of the peri-Gondwanan terrane exposed between the Central Unit and the South-Portuguese Zone of the Iberian Massif (i.e., most of the Ossa-Morena Zone defined by *Lotze*, 1945 and *Julivert et al.*, 1972) (*Díez Fernández and Arenas*, 2015). The structural analysis presented in this work supports the rootless nature of a suture zone exposure affected by a strike-slip shear zone formed during transpression and allows re-consideration of lower and upper plates. The Variscan Orogen is divided in tectonic blocks bounded by strike-slip faults (Fig. 2) that cut across the nappe stack structure of the orogen (e.g., *Faure et al.*, 2008; *Martínez Catalán et al.*, 2020; *Matte*, 2001; *Schulmann et al.*, 2014). Consequently, other suture zone exposures along the Variscan Orogen may similarly be rootless.

2. GEOLOGICAL SETTING

The Variscan Orogen resulted from the collision of Laurussia, Gondwana and their peripheral terranes after the consumption of the Rheic and other subsidiary oceans (Fig. 2; *Díez Fernández et al.*, 2016; *Faure et al.*, 2008; *Franke*, 2000; *Kroner and Romer*, 2013; *Martínez Catalán et al.*, 2009; *Matte*, 2001; *Simancas et al.*, 2013), as part of the amalgamation of Pangea in the late Paleozoic. The Iberian Massif is a crystalline basement that records many of the processes that took place during the Variscan Orogeny (Fig. 3). These processes include the establishment of the subduction zones that consumed the existing Paleozoic oceans (*Díez Fernández et al.*, 2012; *Gómez Barreiro et al.*, 2010), syn-collisional regional-scale thrusts and folds (*Azor et al.*, 1994; *Díez Fernández et al.*, 2011; *Martínez Catalán et al.*, 1996), post-collisional orogenic collapse (*Escuder Viruete*

et al., 1994; *Martínez Catalán et al.*, 2002; *Pereira et al.*, 2009), development of strike-slip shear zones (*Díez Fernández and Pereira*, 2017; *Iglesias Ponce de Leon and Choukroune*, 1980; *Llana-Fúnez and Marcos*, 2001) and oroclinal bending of the entire orogen (*Weil et al.*, 2013) and coeval magmatism (*Fernández-Suárez et al.*, 2011) that culminated or followed the Variscan record.

The Iberian Massif hosts several suture zone exposures. Some of them have been identified as Cadomian (Neoproterozoic-Cambrian in age) (*Arenas et al.*, 2018; *Díez Fernández et al.*, 2019; *Díez Fernández et al.*, 2021), while others are Variscan (*Abati et al.*, 2018; *Arenas et al.*, 2016; *Azor et al.*, 2008; *Moita et al.*, 2005; *Pereira et al.*, 2010a; *Rosas et al.*, 2008). A classical view for the Variscan examples is that almost all suture zone exposures are interpreted as recording separate and distinct subduction zones. One example is the Central Unit, which is thought to represent the root zone of a suture separating an upper plate to the NE from a lower plate to the SW (*Azor et al.*, 1994; *Burg et al.*, 1981; *Pereira et al.*, 2010a).

The Central Unit is a high-P metamorphic belt (*Abalos et al.*, 1991a) formed in a Devonian subduction zone (*Abati et al.*, 2018; *Azor et al.*, 1994). This belt is bound to the north by the Matachel Fault (*Azor*, 1994) and to the south by the Azuaga Fault (*Chacon et al.*, 1974) (Fig. 3). The Matachel Fault is a NE-dipping sinistral strike-slip fault with normal oblique-slip movement, whose hanging wall exposes the upper plate (Obejo-Valsequillo Domain) of a Devonian subduction zone (Central Unit) (*Azor*, 1994; *Azor et al.*, 1994). Some studies consider this fault to have reverse oblique-slip movement (*Abalos and Eguiluz*, 1991; *Ábalos*, 1990), but other works point to a down-thrown movement for the hanging wall, which is consistent with the metamorphic contrast across the Matachel Fault with the Central Unit on the footwall (*Azor*, 1994; *Azor et al.*, 1994; *Simancas et al.*, 2003). The Azuaga Fault is also a sinistral strike-slip fault for which

either reverse oblique-slip (*Abalos and Eguiluz*, 1991) or normal oblique-slip (*Azor*, 1994) motions have been proposed. The geometry of the Azuaga Fault is disputed. *Abalos and Eguiluz* (1991) proposed a NE-dipping geometry for the Azuaga Fault, whereas Azor (1994) considered it as near-vertical.

The Central Unit is comprised of a variety of gneisses, schists and metabasites (*Abalos et al.*, 1991a; *Azor*, 1994; *Pereira et al.*, 2010a). Some protoliths of its metasedimentary rocks are Ediacaran in age and were deposited along the periphery of Gondwana (*Pereira et al.*, 2010a). To the north of the Matachel Fault and within the Obejo-Valsequillo Domain (Fig. 3), the evolution of metasedimentary and metaigneous rocks can be divided in two tectonic stages: pre-orogenic and Variscan (syn-orogenic). The pre-orogenic stage consists of Ediacaran to Devonian rocks deposited or intruded in peri-Gondwanan basins related to the onset of a Cadomian arc and subsequent passive margin conditions in the Paleozoic (*Martínez Poyatos*, 2002; *Rojo-Pérez et al.*, 2019; *San José et al.*, 2004). The syn-orogenic stage consists of Carboniferous rocks that unconformably overlie rocks of the pre-orogenic series (*Martínez Poyatos et al.*, 1998b). Variscan deformation in the pre-orogenic stage rocks includes NE-directed thrusts and NE-verging folds. Normal and strike-slip faults, and upright folds affected both pre-orogenic and syn-orogenic rocks (*Ábalos*, 1990; *Martínez Poyatos et al.*, 1995, 1998a). Syn-orogenic rocks are characterized by low- to very-low grade metamorphism, and pre-orogenic rocks by Variscan low-grade metamorphism (e.g., *Martínez Poyatos et al.*, 2001).

Bedrock to the south of the Azuaga Fault can be also divided into pre-orogenic and syn-orogenic rocks. We describe the sections that are close to (< 10 km) and located SW from the Azuaga Fault (colored in green and yellow in Figure 3). Pre-orogenic rocks include Ediacaran to Devonian strata and Ediacaran to Ordovician igneous rocks that

formed along the periphery of Gondwana, initially related to a continental arc that is part of the Late Neoproterozoic – Early Cambrian Avalonian-Cadomian belt (Ediacaran to Cambrian rocks; *Arenas et al.*, 2018; *Eguíluz et al.*, 2000; *Quesada*, 1990), and the Late Cambrian – Early Ordovician establishment of a passive margin during the opening of the Rheic Ocean (Cambrian to Devonian rocks; *Robardet and Gutiérrez Marco*, 2004; *Sánchez-García et al.*, 2003). The Variscan syn-orogenic rocks consist of Devonian to late Carboniferous sedimentary and igneous rocks. Variscan deformation is dominated by SW-verging folds and thrusts (which affect both pre- and syn-orogenic successions), followed by normal and strike-slip faults, and coeval upright folds (*Díez Fernández et al.*, 2019; *Eguiluz et al.*, 1990; *Expósito et al.*, 2002). Variscan metamorphism ranges between low-grade (especially in the green section of Figure 3; *Expósito Ramos*, 2005) and medium-grade (some parts in the yellow section of Figure 3; *Azor and Ballèvre*, 1997; *Garrote*, 1976; *González del Tánago and Arenas*, 1991).

3. MATERIALS AND METHODS

Geological mapping was performed at the 1:25,000 scale using a rugged tablet computer and GIS software. Topographic maps and digital orthophotos from the Spanish National Geographical Survey (http://centrodedescargas.cnig.es) were used as base maps for construction of the geologic map. Orientation of structural data was obtained with traditional analog compass. Statistical analysis of structural data was done with Stereonet (*Cardozo and Allmendinger*, 2013).

Transpressional shear zones have been modeled using analytical (e.g., *Dewey et al.*, 1998; *Fossen and Tikoff*, 1993, 1998; *Jones et al.*, 2004; *Lin et al.*, 1998), numerical (e.g., *Braun*, 1993; *McCaffrey et al.*, 2000; *Nabavi et al.*, 2020; *Vernant and Chéry*, 2006), and analog models (e.g., *Casas et al.*, 2001; *Leever et al.*, 2011; *McClay et al.*, 2004;

Richard and Cobbold, 1990). Transpression can be seen as a three-dimensional flow regime in a high strain zone that combines simple shear parallel with the shear zone boundaries, and coaxial flow resulting from shortening across the zone. Transpression flow can be monoclinic or triclinic. A flow is triclinic when the infinitesimal vorticity vector is oblique to the three instantaneous stretching axes (ISA; *Passchier*, 1997), and ISA orientations are not necessarily fixed in an external reference frame (e.g., the boundaries of the shear zone). Most kinematic models of transpression consider homogeneous, steady-state flow. Although the deformation in nature is commonly heterogeneous, the study area is usually divisible into smaller domains within which the homogeneity of the deformation is assumed (e.g., *Fossen and Tikoff*, 1998; *Ramsay and Graham*, 1970). More debatable is the assumption of steady flow. However, deformation paths are rarely known and steady deformation can be a valid approximation, particularly if constant boundary conditions persisted during the activity of the shear zone (e.g., *Fossen and Tikoff*, 1997; *Jiang et al.*, 2001; *Tikoff and Fossen*, 1995).

The transpressional character of the Azuaga Fault is here evaluated using an analytical model of triclinic transpression with oblique extrusion (*Fernández and Díaz-Azpiroz*, 2009). In this model, the main parameters controlling the flow pattern within the shear zone are: (1) the transpression obliquity, defined by angle ϕ, i.e., the angle between the simple shear direction and the strike of the shear zone, (2) the angle υ between the extrusion direction, related to the coaxial component of flow, and the dip direction of the shear zone, (3) the relative amount of the simple shearing component with respect to the coaxial component, characterized by the kinematic vorticity number, W_k (*Truesdell*, 1953). W_k values vary between 1 (simple shearing) and 0 (coaxial flow). The model can consider any type of coaxial component, although in this work a pure shear component has been sufficient to adequately simulate the structures and fabrics observed in the

Azuaga Fault. The model is able to deal with virtually any of the most common types of transpressional flow, either monoclinic or triclinic, and also with zones characterized by inclined boundaries. For specific values of its controlling parameters (among other structural features), the model can determine the shape and orientation of the strain ellipsoid, the shape of the resulting folds, the magnitude of extrusion parallel to the boundaries of the shear zone, and the orientation of the convergence vector between the blocks separated by the shear zone. A protocol was developed to check the model against natural ductile and ductile-brittle shear zones (*Díaz-Azpiroz et al.*, 2014; *Fernández et al.*, 2013), mainly comparing the finite strain produced by the model against the fabrics and other finite strain structures observed in the studied natural case.

4. THE AZUAGA FAULT ZONE

Reference Points (referred to in the text as RP-1, RP-2, etc.) are used for clarity in data description and located using circled numbers in Figure 4a.

4.1. Fault zone and subsidiary faults

The Azuaga Fault (RP-1; Fig. 4a) strikes WNW-ESE (N108ºE on average), with some minor variation in its trend to the north of Berlanga village, and juxtaposes the Central Unit against Cambrian and Carboniferous rocks. The fault zone is characterized by cataclasites, breccias and gouges (Fig. 5a). Breccias and gouges within the zone (see further description by *Ábalos*, 1990) vary in width from < 10 m to > 300 m, occur in both hanging wall and footwall rocks, and make up > 50% of the rock volume. Most faults within the zone strike NW-SE and dip between ~55º and ~75º (61ºNE on average) (Figs. 4a, 4b, 4c, 4d, 4e, 5a). The fault trace V pattern apices point NE up drainages on very

gentle SW-facing slopes, indicating moderate to steep NE dips for the Azuaga Fault. A good example of that can be seen to the W of Azuaga village (RP-2; Fig. 4a).

The trace of the Azuaga Fault merges with subsidiary faults, which collectively define an imbricate structure. Two minor faults stand out, namely Berlanga-1 Fault (RPs-3-4-5; Fig. 4a) and Berlanga-2 Fault (RPs-6-7; Fig. 4a). Berlanga-1 Fault is also marked by breccias and gouges (fault zone is ~15 meters in thickness) and shows similar NE-dipping geometry to the Azuaga Fault, if slightly less inclined in some areas (note pronounced V-shapes of its trace NE of Berlanga village; Fig. 4a). Berlanga-2 Fault is near-vertical and its fault includes gouges, breccias and phyllonites (Fig. 5b). The Azuaga and Berlanga-1-2 faults step to the right as you move along strike to the northwest of Berlanga village, where the number of minor faults seems larger than elsewhere. The Berlanga-1-2 faults, along with many other minor faults, depict a series of connecting imbricates (e.g., RPs-8-9; Fig. 4a) and horses (e.g., RP-10; Fig. 4a). The strike of minor faults is generally clockwise from the major faults (Fig. 4e).

Fault planes may show slickenlines (Fig. 5c) and slickenfibres (Fig. 5d), which trend E-W in the Azuaga Fault, NW-SE in the minor faults and plunge shallowly to the E (Fig. 4e), except for the Berlaga-2 Fault, where they are sub-horizontal. The stepped structure of slickenlines (Fig. 5c) and slickenfibres (Fig. 5d) indicates consistent sinistral shear sense for all faults, consistent with kinematics constrained by CS fabrics in cataclasites, breccias (Fig. 5e) and phyllonites (Fig. 5b), and by sigma porphyroclast structures in phyllonites/cataclasites (Fig. 5f).

4.2. Fault blocks

4.2.1. Lithostratigraphy

The hanging wall to the Azuaga Fault consists of albite-bearing schists and paragneisses (Fig. 6a), migmatitic paragneisses, metasandstones, black quartzites, metabasites (retroeclogites; Fig. 6b), and felsic to intermediate orthogneisses (Fig. 6c). This rock ensemble comprises the Central Unit (*Azor et al.*, 1994), and the protoliths of some of its metasedimentary rocks are Ediacaran in age (*Pereira et al.*, 2010a).

The footwall to the Azuaga Fault is comprised of pre-Variscan and Variscan (syn-orogenic) units. The pre-orogenic units include a series of mica-schists and metasandstones (Albariza-Bembézar Succession; *Delgado Quesada*, 1971; *González del Tánago*, 1995), and micro-banded phyllites (Fig. 6d) and metasandstones (Azuaga Formation; *Apalategui et al.*, 1983; *Delgado Quesada*, 1971). The depositional age of the Azuaga Formation protoliths is Early-Middle Cambrian (*Jensen et al.*, 2004; *Liñán*, 1978), and the age of the Albariza-Bembézar Succession, which rests on top of Paleozoic strata (*Azor et al.*, 1991; *Marcos et al.*, 1991) and below the Azuaga Formation, is inferred to be Early Cambrian.

Syn-orogenic metasedimentary rocks include meta-conglomerates (Fig. 6e), meta-sandstones, slates and minor meta-limestones and coal. The meta-conglomerates contain irregularly-shaped and -sized clasts of micro-banded phyllites similar to those of the Azuaga Formation. The basal part of this syn-orogenic series has been estimated at late Tournaisian – early Visean in age (*Gabaldón et al.*, 1985; *Hartung*, 1941). Syn-orogenic igneous rocks are represented by a rhyolitic dike intruded along the Berlanga-2 Fault, which contains xenoliths of foliated rocks and black quartzites (Fig. 6f).

4.2.2. Internal structure in the hanging wall

The metamorphic rocks of the Central Unit are characterized by a S_2 penetrative, post-eclogitic and mylonitic foliation that is parallel to bedding (Fig. 6a) and to the

elongate shape of orthogneiss bodies (Fig. 4a). This S_2 foliation post-dates the first phase (D_1) of deformation recorded in this unit, which is interpreted to reflect subduction down to high-P metamorphic conditions (*Abalos et al.*, 1991a; *Arenas et al.*, 2020; *López Sánchez-Vizcaíno et al.*, 2003) during the Devonian period (*Abati et al.*, 2018). D_2 deformation and generation of the main (S_2) foliation in the Central Unit occurred in the early Carboniferous during post-eclogitic recrystallization (D_2) (355-340 Ma; *García Casquero et al.*, 1988; *Pereira et al.*, 2010a) under amphibolite to greenschist facies conditions (6-12 kbar; *Abalos et al.*, 1991a; *Arenas et al.*, 2020; *Pereira et al.*, 2010a) (see individual descriptions of S_2 for each lithology by *Ábalos*, 1990; *Azor*, 1994).

S_2 is deformed into upright NW- to SE-plunging periclinal folds (D_3; Fig. 6c), as are the different bodies of gneiss (Figs. 4a, 4b, 4c, 4d); the change in plunge direction from NW (e.g., RPs-11-12; Fig. 4a) to SE (e.g., RP-13; Fig. 4a) is localized over the section where major faults have a trace with an inflexion (RP-1; Fig. 4a). This change is also noticeable from the folded structure shown by S_2 (Fig. 7), which presents changing plunges from west (Fig. 7a) through to east (Fig. 7d). In the hanging wall to the Azuaga Fault, D_3 upright folds are accompanied by an axial plane crenulation cleavage (S_3; Fig. 6a) (Fig. 4g) defined by neoblastic quartz, muscovite, sericite and chlorite, as well as reoriented minerals from previous fabrics. The strike of S_3 is oblique and mostly clockwise relative to that of the Azuaga Fault (Fig. 4f, 4g). D_3 axial planes calculated (following *Cardozo and Allmendinger*, 2013) from S_2 measurements are near-vertical, steeply dipping to the NE (Fig. 7) and parallel to S_3 (Fig. 4g). S_3 contains a mineral lineation ($_mL_3$) defined by muscovite, chlorite and sericite. $_mL_3$ trends NW-SE and consistently plunges gently to the SE (Fig. 4g). The S_3 mineral assemblage formed under greenschist facies conditions (2-5 kbar; *Abalos et al.*, 1991b). S_3 affects granitoids dated

at 318 Ma (*Pereira et al.*, 2010b) and is cut by granitoids dated at 306 Ma (*Solá et al.*, 2009), so S_3 is late Carboniferous (Pennsylvanian).

The majority of S_2 planes dip to the SW within 1-3 km of the Azuaga Fault (between 22º-70º; mean at ~55º) (e.g., surroundings of RP-13; Fig. 4a) and is near-perpendicular to the NE-dipping geometry of the Azuaga Fault (Figs. 4b, 4c, 4d). However, to the NE, S_2 is NE-dipping thus defining a regional upright D_3 antiform in the hanging wall to the Azuaga Fault (Fig. 6c) (*Chacón*, 1982). These folds are periclinal, as depicted by lithological contacts observed in several sections (RPs-11-12; Fig. 4a), although in some sections this regional antiform includes parasitic folds across its hinge zone (e.g., RP-13; Fig. 4a). The obliquity between the Azuaga Fault and the internal structure of its hanging wall is also evident from the mapping of the elongate bodies of orthogneiss that can be mapped in the southwestern limb of the antiform that is cut by the fault (RPs-2-12-14; Fig. 4a). The steeper dip of S_3 compared to the Azuaga Fault implies they are oblique, some 27º (Fig. 4g). Upright D_3 fold traces are cut by the Azuaga Fault. This obliquity in strike is low (almost parallel) close to the fault zone but increases up to be ~40º away from it.

4.2.3. Internal structure in the footwall

The syn-orogenic rocks rest unconformably upon the Azuaga Formation (RP-15; Fig. 4a) as bedding and the main foliation in the pre-Variscan rocks are typically oblique to bedding in the unconformably overlying strata. The main foliation in the pre-Variscan units of the footwall to the Azuaga Fault (S_x) is penetrative, but defined by different mineral assemblages in each unit. In the Albariza-Bembézar Succession, this fabric is a schistosity that includes quartz (frequently as lens-shaped segregates), white mica, biotite, plagioclase, and variable amounts of andalusite and garnet. Bedding is rarely preserved.

In the Azuaga Formation, bedding is readily recognizable and the main foliation is a slaty to phyllitic cleavage (Fig. 6d) characterized by relatively fine grained quartz (sometimes in lens-shaped segregations), albite, white mica, chlorite, and minor biotite and garnet. The Azuaga Formation rested structurally above the Albariza-Bembézar Succession before imbrication by the Azuaga Fault. These relationships are indicated by the relative orientations of their respective main foliations and the bedding observed within the horses of the fault imbricates (e.g., RP-10; Fig. 4a). The contact between the Azuaga Formation and the Albariza-Bembézar Succession before this imbrication is tentatively considered as an extensional detachment, which juxtaposed these sequences with contrasting (low grade-high-grade, respectively) metamorphic assemblages. Equivalent extensional faults separating these series have been identified in the region, such as the Casa del Café Fault (*Azor*, 1994).

The bedding and main foliation of the rocks in the footwall to the Azuaga Fault are affected by upright folds (Fig. 8a), which show similar geometry to the D_3 folds in the hanging wall, including a NW-SE periclinal folds with steeply NE-dipping axial planes (Fig. 7). The axial plane foliation (S_3) varies between an anastomosing spaced (Fig. 8b) and a regularly spaced cleavage (Fig. 6e) in the metaconglomerates, and between a spaced (Fig. 8c) and a crenulation cleavage (Fig. 6d) in slates and phyllites. S_3 occurs throughout the footwall to the Azuaga Fault (Fig. 4f), and has both a similar mineralogy and a similar orientation to S_3 in the hanging wall (NE-dipping and clockwise from the strike of the Azuaga Fault).

The syn-orogenic deposits are preserved in the cores of D_3 synforms (e.g., RPs-16-17; Fig. 4a), which are separated by anticlinoria cored by pre-Variscan rocks (RP-7). The fault imbricates related to the Azuaga Fault, and the latter fault itself show the following pattern: the first major D_3 fold located NE from the fault is an antiform and the

first major D_3 fold SW from the fault is a synform. This pattern can be also observed at the outcrop scale, where minor thrusts directed to the SW cut across the forelimb of paired and slightly asymmetric SW-verging D_3 folds (Fig. 8d).

The axial trace of D_3 folds in the pre-Variscan rocks is oblique to the base of the syn-orogenic rocks, which overlie different fold limbs from east to west (e.g., RPs-15-18; Fig. 4a). The obliquity of the Azuaga Fault and its imbricates with the internal structure of its footwall is evident from the crosscutting relationship between these faults and the internal contacts between both the syn-orogenic rock (RPs-7-19; Fig. 4a) and the pre-Variscan rock units (RP-10; Fig. 4a). Upright D_3 fold traces in the footwall are commonly cut by the Azuaga Fault and its imbricate faults. The S_3 axial surface typically dips to the NE, but locally can also be near-vertical or dip to the SW (Fig. 4f), depicting in all the cases a steeper and oblique geometry compared to that of the Azuaga Fault and its imbricates (Fig. 4g).

5. KINEMATIC ANALYSIS

The entire study area has been kinematically analyzed synoptically, i.e. without a division into sectors for which there is not enough information. As a result, only a first approximation has been reached to the kinematic description of the transpressional flow responsible for the observed deformation. The analyzed structure includes the complex trace of the Azuaga Fault itself, as well as the part of the hanging wall (Central Unit) and footwall blocks shown in Figure 4. The structures described here suggest that the primary strike-slip faults of the studied segment of the Azuaga Fault acted as structures that absorbed the simple shear component (that is, $W_k \approx 1$), whereas the blocks bounded by them could have undergone a more general transpressional flow (i.e. $W_k < 1$). Accordingly, the mean orientation of the primary strike-slip faults (N108ºE/61ºNE, Fig.

4) has been used as indicative of the average attitude of the boundaries of the entire deformation zone. The slickenlines and slickenfibers measured in the primary faults allow the pitch of the simple shear direction on the shear plane to be obtained (angle ϕ), which is ca. 19.2º SE (95% confidence cone with a half-angle $-\alpha_{95}$- of only 4.2º). The slip sense associated with the simple shearing component is sinistral-reverse, as shown in this work. In order to apply the transpression model to constrain the flow parameters controlling the kinematic history of the domains limited by the primary faults, a wide range of extrusion angles have been considered (υ = 0º, 10º, 15º, 19.2º, 25º, 30º, 40º, 50º, 70º, 90º, 109.2º, 140º, 170º; see Figure 9a for information about the location of the extrusion direction along the shear zone boundary for those values of angle υ). Although, in theory, any kinematic vorticity number could explain the flow in the domains between the strike-slip faults, a first study has allowed all the values of $W_k < 0.7$ to be discarded, because, in those cases, the plunge of the lineations predicted by the model would be much steeper than those measured in the field. Therefore, the vorticity values explored in detail are: W_k = 0.7, 0.81, 0.9, 0.95, 0.99, 0.9999. Most values are in the field of simple-shearing dominated flow ($\geq$ 0.81, according to e.g., *Fossen and Tikoff*, 1993).

The orientation of the trajectories of the principal finite strain axes for the distinct combinations of the controlling parameters described above (ϕ, υ, W_k) is then represented in stereoplots and compared with the distribution of the D_3 fabrics. The poles to the mean S_3 foliation and the $_mL_3$ lineations are compared with the orientation of the *Z* and *X* axes of the predicted finite strain ellipsoid, respectively (see the entire set of stereoplots with the comparison between the results of the model and measured data in the Supplementary Material). The best fit to the natural data is obtained for the following range of the kinematic parameters (Figure 9a shows the case for υ = 50º): (1) υ = 30º to 50º; (2) W_k = 0.9 to 0.99. Therefore, the simple shear and the extrusion directions are not normal and

not coincident, and the transpression flow is triclinic. Furthermore, deformation can also be proved to be the result of a triclinic flow if the angle between the measured lineation and the intersection of the shear zone boundary and the foliation deviates from either 0º or 90º (*Jones et al.*, 2004). This deviation is seen from the data collected (Fig. 9b), thus supporting the results of the kinematic modeling.

Due to the absence of adequate markers or appropriate data to determine the shape of the finite ellipsoid, it is not possible to further check the Azuaga Fault against the kinematic model of transpression (see e.g., *Díaz-Azpiroz et al.*, 2014; *Fernández et al.*, 2013). Therefore, the range of model parameters that has been obtained here cannot be further constrained.

6. DISCUSSION

The detailed geometric and kinematic characterization of the Azuaga Fault as a triclinic transpressional shear zone, as presented in this work, is a necessary condition to: (1) understand the progressive development of the set of structures and tectonic fabrics associated with the activity of the shear zone, (2) establish the direction of relative convergence between the blocks separated by the shear zone, (3) estimate the exhumation rates associated with the extrusion kinematic component, and (4) reconstruct with precision the geometry and original attitude of the structures prior to activity in the shear zone, with the consequent implications in the understanding of the tectonic evolution of the orogenic belt. All of these topics will be explained in more detail throughout this discussion.

6.1. Interpretations of the kinematic model

Although there are no robust indications about the shape of the D_3 deformation ellipsoid in the domains located between the strike-slip faults, the widespread presence of planar fabrics (S_3) and the lower abundance of lineations ($_mL_3$) suggest oblate (flattening) ellipsoids. The results of the model agree with that interpretation. The finite strain ellipsoids predicted for the best-fit results plot in the field of flattening ellipsoids (Fig. 9c). For the larger vorticity values (W_k = 0.99), the strain paths are closer to the plane-strain ellipsoid line, deviating from this line with increasing strain intensity.

The convergence vector between the blocks separated by the deformation zone is marked by the flow apophysis oblique to the boundaries of that zone (e.g., *Fossen and Tikoff*, 1998). The flow apophyses or asymptotes are the eigenvectors of the gradient-velocity tensor (e.g., *Passchier*, 1997). Determination of the oblique flow apophysis for the best-fit values obtained in this work for the Azuaga Fault indicates a convergence direction, in present coordinates, between N77ºE and N92ºE, gently plunging to the E (Fig. 9d). This convergence direction should be taken into account in any interpretation concerning the tectonic setting and evolution of the studied region during the D_3 phase.

Another implication of the kinematic study is the possibility to constrain the amount of vertical extrusion due to the coaxial flow component (note that this figure does not consider the exhumation due to the dip-slip, simple shearing component). The amount of extrusion depends on the strain rate, the amount of time of steady activity of the transpressional zone, and the initial distance of the studied rock volume above a rigid floor depth, taken as a reference level (*Schulmann et al.*, 2003). Given the range of υ angles (extrusion obliquity) determined in this work (30º to 50º), taking an intermediate value of $\upsilon = 40º$ and reasonable figures of strain rate normal to the shear-zone boundaries of $10^{-14}s^{-1}$ to $10^{-15}s^{-1}$, the vertical extrusion would be of 0.5 to 4.6 km per every million years of activity of the structure. Although this range of exhumation rates was determined

for a reference level of 30 km, it can be predicted that the exhumation values should increase with the depth to the reference level and vice versa. In this sense, a reference level located at a depth of 40 km would yield exhumation rates ranging from 0.6 (for a strain rate of $10^{-15}s^{-1}$) to 6.1 (for a strain rate of $10^{-14}s^{-1}$) km/m.y., while the corresponding range for a reference level of only 15 km varies from 0.2 to 2.3 km/m.y. The estimated exhumation rates are within the same order of magnitude for a given strain rate, irrespective of the considered reference level (15, 30, or 40 km), and explain the metamorphic differences due to D_3 between the Central Unit and the rocks exposed in the footwall to the Azuaga Fault. These exhumation rates can be useful to estimate the depth to the Central Unit (or analogous domains representative of the Devonian suture zone) that lies below the surface at the footwall to the Azuaga Fault. The values of the depth to the reference level considered in this work (15 to 40 km, and particularly the intermediate value of 30 km), assume that the Azuaga Fault is a crustal scale structure. This assumption is firstly based on metamorphic data. S_3 is associated with the Azuaga Fault and formed under greenschist facies conditions, probably in the upper-middle crust (> 6-12 km). After subduction of the Central Unit (D_1), D_2 exhumation proceeded up to 6-12 kbar (*Abalos et al.*, 1991a; *Arenas et al.*, 2020; *Pereira et al.*, 2010a), so D_3 structures such as the Azuaga Fault are responsible for the exhumation of rocks that were localized at middle-lower crust depths. Secondly, seismic images of this region (*Simancas et al.*, 2003) reveal a reflector that coincides with the geometry and location of the Azuaga Fault proposed from surface data in this work and that penetrates to the current middle crust (~12-15 km). Previous works interpreted this reflector as internal structure within the Central Unit (e.g. *Simancas et al.*, 2003). Such internal structure does not reconcile with surface geology data (e.g. Fig. 4). We interpret this seismic reflector as the Azuaga Fault. The depth of the deepest section of the Azuaga Fault is a minimum estimate of its original depth since

D_3 structures probably assisted the exhumation of rocks that were even deeper. The cross-sections made from surface geology suggest a significant part of the Azuaga Fault was lost to erosion (Fig. 4). S_3 in the syn-orogenic rocks of the hanging wall of the Azuaga fault formed under metamorphic conditions of the anchizone-epizone transition (*Abalos et al.*, 1991a), so a minimum of 4 km of crust is missing. In transpressional structures the coaxial extrusion component produces most of the observed exhumation, contrary to the widely held belief that the uplift can be estimated by simple trigonometric calculations from the pitch of the displacement direction on the deformation zone boundary. If that were the case, explaining large vertical uplifts could (in some cases) require displacements of several thousand km, which is unnecessary considering the exhumation due to the coaxial component of extrusion.

Folds are among the most important structures generated by the activity of the Azuaga Fault during D_3. D_3 folds affect all the previous planar fabrics (S_0, and S_x and S_2 foliations), with S_3 as an axial plane foliation. The statistically determined D_3 fold axes (Fig. 7) can be used to gain some insight into the pre-D_3 orientation of the folded planar fabrics. The procedure followed considers folds are formed by layer-parallel shortening, and fold hinges nucleate normal to the maximum instantaneous shortening direction (e.g., *Fossen et al.*, 2013). A wide range of possible original orientations of S_0, S_x and S_2 has been considered from which it is possible to compute, for each orientation of the folded planar fabric, the location of the initial fold hinges using the best-fit values of the transpression model applied in this work. Assuming that fold hinges rotate as material lines, their corresponding theoretical reorientation trajectories can also be determined. The statistical fold axes obtained from the Azuaga Fault are then projected on stereoplots including the computed theoretical trajectories. Those cases where the measured fold axis coincides with a given theoretical reorientation path can be used to infer the original

orientation of the folded fabric (Figs. 10a, 10b, 10c). Note that the folds of the Eastern section have not been included in the procedure, because they do not match the theoretical reorientation trajectories. A possible explanation is that the orientation of the shear zone is more E-W at the Eastern section, thereby deviating from the WNW-ESE trend in the other domains of the structure, triggering local departures in the attitude of fold elements. The estimated original orientation of S_0, S_x and S_2 slightly varies from one section to another. The three planar fabrics were close to the horizontal, although their mean orientations suggest that they were not completely parallel before D_3, and formed average dihedral angles of between 12º and 21º (Fig. 10d). While S_0 was supposedly dipping to the SE (less than 20º), S_x probably had a similar strike although dipping at a steeper angle (Fig. 10d). On the other hand, S_2 could have a NW-SE strike, with rather small dips (<10º) to the SW.

The estimated obliquity between S_0 and S_x suggests that S_x could be an axial plane foliation to folds with SE-dipping axial planes (NW-verging?) that formed before D_3, implying the rocks of the Autochthon are located at the backlimb of one of those folds. In the Azuaga Formation, such fold geometry and relationships to local main foliation are equivalent to those that can be observed in that same unit to the north of the Central Unit (*Díez Fernández et al.*, in press; *Martínez Poyatos et al.*, 1995, 1998a). This is also in agreement with the discordant nature between the Autochthon and syn-orogenic sediments (pre-D_3 folds should exist in the Autochthon) and with the metamorphic grade increasing downward and lacking discontinuities (especially in metamorphic P) within the Autochthon. The SW-dipping geometry of S_2 before D_3 does not conform to models that assume a primary and persistent NE-dipping geometry for the regional foliation in the Central Unit (*Azor et al.*, 1994), but rather suggests that this suture zone was part of a shallow dipping metamorphic belt before D_3 (see further discussion below).

6.2. Kinematic evolution model for the Azuaga Fault

From a geometrical point of view, the Azuaga Fault plus its imbricates and S_3 are similar to the type-I S-C fabrics described by *Berthé et al.* [1979], where S_3 would accumulate finite strain (S-planes) and the faults take localized high shear strain (C-planes) (*Burg et al.*, 1981; *Quesada and Dallmeyer*, 1994). The arrangement of S-C planes at the macro-scale would indicate sinistral sense of shear (Fig. 4g), which is compatible with individual field observations of kinematic criteria within all fault zones (*Abalos and Eguiluz*, 1991; *Azor et al.*, 1994; *Burg et al.*, 1981; *Chacón*, 1979; this work). The line normal to the intersection between S_3 (or calculated D_3 axial planes; S-planes) and fault planes (C-planes) observed over the fault planes is similar in orientation to the slickenlines and slickenfibres in the fault planes (Fig. 4g), and to the orientations of mineral and stretching lineations observed on C-planes of a S-C fabric formed under transpression.

Based on these observations and data, we propose that the Azuaga Fault and its imbricates are part of a major shear zone developed during sinistral transpression (*Ábalos*, 1990; *Azor*, 1994; *Burg et al.*, 1981; *Jackson and Sanderson*, 1992; *Pereira et al.*, 2008; *Pérez-Cáceres et al.*, 2016), where strain would have been partitioned into more discrete shear bands (i.e. the faults) and folded domains. Displacement along strike would be mostly accommodated by faults, whereas sub-horizontal shortening would have been accommodated by the component of reverse dip-slip movement along the faults as well as the generation of D_3 upright folds and associated foliation (S_3) in the hanging wall and footwall. The abundance of subsidiary faults over the section where the Azuaga Fault steps to the right may be explained by the development of a restraining bend.

The cross-cutting relationships between structures preserved in the study area indicate that D_3 shearing occurred under greenschist facies conditions in the upper-middle crust (formation of S_3) and brittle conditions in the upper crust (formation of breccias and gouges). The evolution of the D_3 towards lower temperatures occurred in two overlapping stages: an early stage that featured widespread development of steeply inclined to upright folds and related foliation (S_3), and a later stage where strain was partitioned into discrete domains (faults). This evolution can be explained by degeneration of the velocity field in domains affected by a high simple shear component (non-coaxial laminar flow) (e.g. *Torvela and Ehlers*, 2010). The relationship between steeply inclined to upright folds and faults suggests that the narrow shear bands (i.e. faults) were localized preferentially along the forelimbs of paired, asymmetric, major folds, resulting in regional antiforms in the hanging walls and regional synforms in the footwalls to the faults. In this scenario, S_3 could have acted as a mechanical weakness that facilitated nucleation of the faults, however its obliqueness relative to the faults casts doubt about such an interpretation.

One of the major throws in the region is inferred for the Azuaga Fault, which juxtaposes the eclogite- and migmatite-bearing Central Unit and Variscan low-grade metamorphic rocks, including syn-orogenic Carboniferous strata. The throw of the fault imbricates in the study area are arguably more limited. The Carboniferous syn-orogenic rocks of the northern upright D_3 synform (RP-16; Fig. 4a) are contiguous across the upright fold and fault structure with the syn-orogenic rocks in the southern upright D_3 synform (RP-17; Fig. 4a) via a local occurrence of syn-orogenic deposits located in between them (RP-20; Fig. 4a). Another significant throw was recognized across the Matachel Fault, a NE-dipping extensional fault with sinistral and dip-slip movement in which Variscan low-grade and low-P metamorphic rocks are above the eclogite- and migmatite-bearing Central Unit (*Azor*, 1994; *Azor et al.*, 1994) (Fig. 3). The Matachel

Fault either cuts or is unaffected by the D_3 upright folds within the Central Unit (*Azor*, 1994), a relationship that is also apparent from seismic imaging of this region (*Simancas et al.*, 2003). In this scenario, the Central Unit would be bounded by two NE-dipping, sinistral faults with dip-slip components, the upper fault with normal displacement (Matachel Fault) and the lower one with reverse movement (Azuaga Fault) (Figs. 3b and 11). Similar kinematic patterns within transpressional settings, with an inclined and uplifted block bounded by two deformation zones or faults, one at its base with a reverse dip component, and the other at its top with a normal dip component, have been described (e.g., at the Torcal de Antequera massif by *Díaz-Azpiroz et al.*, 2014, or at the Sanbagawa belt of Japan by *Wallis*, 1998, and *Wintsch et al.*, 1999, among others). Both bounding deformation zones can be considered to be similar to the stretching faults of *Means* [1989], a concept that has been applied to transpression settings (e.g. *Sullivan and Law*, 2007). The faults limiting the Central Unit have been traditionally considered to be part of the Coimbra-Córdoba Shear Zone (*Ábalos*, 1990; *Azor*, 1994; *Burg et al.*, 1981; *Pereira et al.*, 2008), which is one of the major shear zones in the Variscan Orogen (Figs. 2 and 3b). If so, its geometry would be non-vertical and the shear zone would have experienced coeval contraction (S_3 and D_3 folds), strike-slip (e.g., Berlanga-2 Fault) and dip-slip shearing (e.g., Azuaga Fault). Our analysis suggests that the geometrical and kinematic properties of this major fault system fit with those formed under inclined triclinic transpression (*Jones et al.*, 2004) with heterogeneous (partitioned) strain (*Dewey et al.*, 1998), including the expected orientation of foliation (S_3) and stretching/mineral lineation ($_mL_3$) (Fig. 4g) for this type of shear zone. S_3 dips more steeply and strikes obliquely (clockwise) to the boundaries of the (sinistral) shear zone, which is assumed to strike roughly parallel to the major NW-SE faults that formed within it (Fig. 3). The average angle (□) between $_mL_3$ and the intersection of S_3 and shear zone boundary,

measured in the plane of the foliation is ~82º (Figs. 4g and 9b), within the range for triclinic strain (*Jones et al.*, 2004).

Transpressional shear zones may experience inclined extrusion of its core due to zone-normal shortening favored by pure shear (e.g., *Fernández and Díaz-Azpiroz*, 2009; *Jones et al.*, 2004). In the study area, the normal and reverse movement of the faults on top and below, respectively, imply the Central Unit is a piece of upward and laterally extruded upper-middle crust (deformation conditions for S_3) that underlies the domains that now flank this high-P unit to the NE and SW. The model of extrusion during inclined transpression only accounts for the latest pulse of exhumation (D_3) of the Central Unit, the older tectonic fabrics being related to earlier exhumation from eclogite facies conditions to the lower-middle crust (not addressed in this work; see *Abalos et al.*, 1991a; *Azor et al.*, 1994).

Some of the structures observed within the fault zone of the Azuaga Fault to the NW of the study area, such as S- to SW-dipping fault planes and slickenlines, indicate dextral and normal dip-slip kinematics for some sections of this fault (*Azor*, 1994). Given the consistent juxtaposition of the Central Unit against lower grade rock assemblages along the entire trace of the Azuaga Fault, we believe the normal dip-slip movement represents a local reactivation of this fault, and that total offset is dominated by earlier reverse faulting that accompanied left-lateral slip.

6.3. Implications for the Variscan Orogen

The quasi-orthogonal cross-cutting relationship between D_2 and D_3 structures suggests that D_3 structures such as the Azuaga Fault do not represent progression of former major tectonic processes and structures (i.e. D_1 and D_2). The ages of deformation do not support such a progression either because D_3 is ~20-25 m.y. younger than D_2.

Finally, D_3 structures cross-cut almost orthogonally syn-orogenic strata that was unconformably deposited on top of the Azuaga Formation and probably the Central Unit (see discussion below). Therefore there is a gap of ~30 m.y. between the late Tournaisian – early Visean sedimentation of the syn-orogenic rocks and the onset of D_3 in Moscovian times, including the development of a sedimentary basin.

The Azuaga Fault is commonly considered to be a re-activated earlier thrust with strike-slip and dip-slip movement and limited vertical throw (*Abalos et al.*, 1991c; *Azor et al.*, 1994; *Chacon et al.*, 1974). If so, the Azuaga Fault should not produce a regional disruption in the pre-fault structure of the region. Instead, our data suggest the Carboniferous syn-orogenic strata rest unconformably above the Azuaga Formation towards the southwest but are overridden by the Central Unit (via Azuaga Fault) towards the northeast. These relationships imply that either the Central Unit and Azuaga Formation were juxtaposed and at the same crustal level and both covered by Carboniferous syn-orogenic strata before motion along the Azuaga Fault (Figs. 12a and 12b), or the Central Unit was located beneath the Azuaga Formation and Carboniferous syn-orogenic strata before that motion along the Azuaga Fault (Fig. 12c).

In the first case, the Carboniferous strata could have covered a former major mechanical contact (a suture zone boundary) between the Central Unit and Azuaga Formation (Fig. 12a). However, this model fails to explain the marked obliquity between the NE-dipping Azuaga Fault and the consistently SW-dipping main foliation within the Central Unit near its fault zone (Figs. 4a, 4b, 4c, 4d). Such a relationship suggests that the Azuaga Fault cut the internal fabrics of the Central Unit (S_2) and its major tectonic boundaries at a moderate to high angle. Therefore, the Azuaga Fault does not seem to be the result of mere reactivation of a former basal boundary of the Central Unit that was parallel to its internal foliation (Fig. 12a), as expected for a major accretionary thrust that

transported the Central Unit onto its relative autochthon located in the lower plate during a Devonian subduction. Even if the Azuaga Fault is a reactivated structure other than a major accretionary thrust, its primary geometry would be markedly oblique to the pre-D_3 internal structure of the suture zone (Fig. 12b), implying that the Central Unit belongs to a Variscan suture zone that must extend to the SW in the footwall to the Azuaga Fault.

A third case implies that before the development of the Azuaga Fault, a section of the Azuaga Formation was located on top of the Central Unit, and that at least the Azuaga Formation was exposed at the surface before the Azuaga Fault moved (Fig. 12c). This model is in agreement with the sedimentary record of the Carboniferous syn-orogenic strata, as they contain a significant proportion of pebbles extracted from an already exposed Azuaga Formation and deposited, after rather limited transport, onto the same formation. The Azuaga Formation was probably exposed towards the south of the Azuaga Fault because there are Carboniferous sediments that lie unconformably on top of it (Fig. 4a). To the north of the Azuaga Fault, a model that accepts that the Azuaga Formation lied on top of the Central Unit before the Azuaga Fault moved would explain a proximal source of Azuaga Formation pebbles derived from the relief created by the Azuaga Fault or other faults. The first option requires that the functioning of the Azuaga Fault and the Carboniferous syn-orogenic strata of this basin be coeval. The age of the basal part of this basin is Tournaisian (*Gabaldón et al.*, 1985; *Hartung*, 1941), whereas the activity for this type of faults and related (D_3) folds in the Iberian Massif is Moscovian through to Gzhelian (*Díez Fernández et al.*, 2016). Consequently, although the Azuaga Fault might have played a role in the latest infilling of this basin, this fault together with other subsidiary faults, are likely cutting across the internal structure of a much larger basin. This relationship can be inferred from the close occurrence of syn-orogenic strata in the core of upright D_3 folds and separated by superimposed faults, from the Azuaga Fault to

the southwest (RPs-5-16-20; Fig. 4a). The second option requires structures able to create relief during the Tournaisian. The onset of the Espiel thrust matches that age (*Martínez Poyatos et al.*, 1995, 1998b), and has been recently considered as a structure that roots to the SW, beyond the exposures of the Central Unit, and responsible for the overriding of the Azuaga Formation onto a Devonian suture zone (*Díez Fernández et al.*, in press). Motion along the Espiel thrust, or along another fault similar to it, would explain the juxtaposition of the Azuaga Formation onto the Central Unit before the Azuaga Fault moved.

The crosscutting relationship between the Azuaga Fault and the internal structure of the Central Unit (Fig. 12d) provides one simple inference: the Central Unit, or some other analogous exposures of this Devonian suture zone, should occur somewhere to the S, SW, and/or W of the Azuaga Fault, and in particular, beneath rocks that are currently exposed in the upper parts of its footwall. This latter position is occupied by a vast exposure of peri-Gondwanan rocks affected by Variscan metamorphism that only reached low-grade and low- to medium-P conditions. This metamorphic fingerprint is compatible with an upper plate position during the Devonian subduction of the Central Unit. Interestingly, the Escoural Unit (*Chichorro*, 2006; *Díez Fernández et al.*, 2017) and the Cubito-Moura Unit (*Araújo et al.*, 2005) (Fig. 3) are comprised of high-P rocks metamorphosed during the Devonian period (*Moita et al.*, 2005; *Rosas et al.*, 2008). Similarly to the Central Unit, the Escoural and the Cubito-Moura units are located beneath the same set of peri-Gondwanan rocks that experienced Variscan low-grade and low- to medium-P metamorphism, and therefore can be interpreted as domains within the Devonian suture zone that should occur south to the Azuaga Fault and related to the Central Unit (*Díez Fernández and Arenas*, 2015).

Our interpretation challenges the traditional understanding of the Variscan Orogen in Iberia because the current location of the Central Unit does not represent the root zone of a Devonian suture zone, but instead is a section of a suture zone underlying SW Iberia that was cut and transported upwards in the hanging wall to the Azuaga Fault (e.g. Fig. 1f). In this model, pieces of the upper plate to the Devonian continental subduction where the Central Unit was involved could occur to the NE and SW of this unit (e.g. Figs. 1f, 1g, and 1h).

7. CONCLUSIONS

The Azuaga Fault is the southern boundary of the Central Unit. It is a high-angle, NE-dipping, strike-slip fault with left-lateral and reverse components that formed during the Pennsylvanian (~315-300 Ma; Moscovian through to the Gzhelian) sinistral transpression. Its markedly oblique geometry relative to former exhumation-related structures in the Central Unit as well as its relative autochthon suggests it is a Variscan breaching fault. The Azuaga Fault is paired with coeval late Variscan folding and fabric development in its hanging wall and footwall and with the Matachel Fault. These relationships support a model in which the latest exhumation of a piece of a Devonian suture (Central Unit) via extrusion from the upper-middle crust occurred under inclined triclinic transpression.

The application of the analytical model of oblique transpression with oblique extrusion to the studied segment of the Azuaga Fault has confirmed that the flow in the domains bounded by primary strike-slip faults corresponds to triclinic transpression, with an extrusion direction plunging to the WNW and a high vorticity ($0.9 \leq W_k \leq 0.99$). The model explains most of the structural characteristics of the Azuaga Fault, as well as the

magnitude of the exhumation experienced during the D_3 phase by its central area, indicating ENE-WSW convergence during this tectonic stage.

The Azuaga Formation occupied an upper structural position relative to the Central Unit before Pennsylvanian faulting. Such a position does not conform to a lower plate position relative to the suture zone exposure represented by the Central Unit, unless undocumented additional thrusting events occurred. The exposed basal contact of the Central Unit should not be considered as the root zone of a Variscan (Devonian) suture zone, but instead is an oblique, NE-dipping high-angle fault that cuts across the suture zone. Therefore, the Central Unit represents an exposure of a Variscan suture zone that underlies the upper plate to the NE and overlies it to the SW, i.e. the Central Unit belongs to a Variscan suture zone that must extend to the SW in the footwall to the Azuaga Fault. Consequently, most of the peri-Gondwanan terrane that is exposed between the Central Unit and the South-Portuguese Zone of the Iberian Massif (most of the Ossa-Morena Zone) is likely underlain by a suture zone that is coeval with the one exposed in the Central Unit, i.e., this suture zone represents the base of a huge continental allochthon emplaced onto mainland Gondwana during the Variscan Orogeny.

This interpretation implies that the major tectonic blocks involved in the Gondwana – Laurussia collision during the Variscan Orogeny need re-appraisal. Late tectonic structures such as the Azuaga Fault have modified the geometry of the suture zones that occur in the Variscan Orogen, whose nappe stack structure of its hinterland is cut by strike-slip faults. Tectonic models that have not recognized the breaching nature of this type of faults should be reconsidered because other suture zone exposures along the Variscan Orogen could not represent the root site of the suture zone they belong to.

8. ACKNOWLEDGMENTS

We are grateful for the comments provided by the editors, Stephen T. Johnston, Brendan Murphy, John Wakabayashi, and an anonymous reviewer. Research funded by Spanish project CGL2016-76438-P (Ministerio de Economía, Industria y Competitividad). Data are available through Díez Fernández et al. (2021).

9. REFERENCES CITED

Abalos, B., and L. Eguiluz (1991), Deformación transpresiva carbonífera en la Zona de Cizalla de Badajoz-Córdoba (Macizo Ibérico meridional), *Revista de la Sociedad Geológica de España*, *4*(3-4), 229-249.

Abalos, B., L. Eguiluz, and J. I. Gil Ibarguchi (1991a), Evolución tectono-metamórfica del Corredor Blastomilonítico de Badajoz-Córdoba. II: Las unidades alóctonas y trayectorias PTt, *Boletín Geológico y Minero*, *102-5*, 617-671.

Abalos, B., L. Eguiluz, and J. I. Gil Ibarguchi (1991b), Evolución tectono-metamórfica del Corredor Blastomilonítico de Badajoz-Córdoba. I: La Unidad Para-Autóctona, *Boletín Geológico y Minero*, *102-4*, 491-523.

Abalos, B., J. I. Gil Ibarguchi, and L. Eguiluz (1991c), Cadomian subduction, collision and Variscan transpression in the Badajoz-Cordoba Shear Belt, Southwest Spain, *Tectonophysics*, *199*, 51-72.

Ábalos, B. (1990), Cinemática y mecanismos de la deformación en régimen de transpresión. Evolución estructural y metamórfica de la Zona de Cizalla Dúctil de Badajoz-Córdoba, PhD thesis, 430 pp, Universidad del País Vasco.

Abati, J., R. Arenas, R. Díez Fernández, R. Albert, and A. Gerdes (2018), Combined zircon UPb and LuHf isotopes study of magmatism and high-P metamorphism of the basal allochthonous units in the SW Iberian Massif (Ossa-Morena complex), *Lithos*, *322*, 20-37.

Abdelsalam, M. G., R. J. Stern, P. Copeland, E. M. Elfaki, B. Elhur, and F. M. Ibrahim (1998), The Neoproterozoic Keraf Suture in NE Sudan: Sinistral Transpression along the Eastern Margin of West Gondwana, *The Journal of Geology*, *106*(2), 133-148.

Allmendinger, R. W., N. C. Cardozo, and D. M. Fisher (2013), *Structural Geology Algorithms: Vectors & Tensors*, 289 pp., Cambridge University Press, Cambridge, England.

Andersen, T. B., B. Jamtveit, J. F. Dewey, and E. Swensson (1991), Subduction and eduction of continental-crust - Major mechanisms during continent-continent collision and orogenic extensional collapse, a model based on the South Norwegian Caledonides, *Terra Nova*, *3*, 303-310.

Apalategui, O., J. Borrero Domínguez, M. Delgado Quesada, F. J. Roldán García, L. Eguiluz Alarcón, L. A. Cueto, and C. Quesada (1983), Mapa Geológico, Hoja 878 (Azuaga), Serie MAGNA, 1/50.000, *Instituto Geológico y Minero de España*.

Araújo, A., P. E. Fonseca, J. M. Munhá, P. Moita, J. Pedro, and A. Ribeiro (2005), The Moura Phyllonitic Complex: an accretionary complex related with obduction in the Southern Iberia Variscan Suture, *Geodinamica Acta*, *18*, 375-388.

Arenas, R., R. Díez Fernández, S. Sánchez Martínez, A. Gerdes, J. Fernández-Suárez, and R. Albert (2014), Two-stage collision: Exploring the birth of Pangea in the Variscan terranes, *Gondwana Research*, *25*, 756-763.

Arenas, R., I. Novo-Fernández, A. Garcia-Casco, R. Díez Fernández, J. M. Fuenlabrada, M. F. Pereira, J. Abati, S. Sánchez Martínez, and F. J. Rubio Pascual (2020), A unique blueschist facies metapelite with Mg-rich chloritoid from the Badajoz-

Córdoba Unit (SW Iberian Massif): correlation of Late Devonian high-pressure belts along the Variscan Orogen, *International Geology Review*, 1-24.

Arenas, R., et al. (2016), Allochthonous terranes involved in the Variscan suture of NW Iberia: A review of their origin and tectonothermal evolution, *Earth-Science Reviews*, *161*, 140-178.

Arenas, R., et al. (2018), The Calzadilla Ophiolite (SW Iberia) and the Ediacaran fore-arc evolution of the African margin of Gondwana, *Gondwana Research*, *58*, 71-86.

Azor, A. (1994), Evolución tectonometamórfica del límite entre las zonas Centroibérica y de Ossa-Morena (Cordillera Varisca, SO de España), 312 pp, Universidad de Granada, Granada.

Azor, A., and M. Ballèvre (1997), Low-pressure metamorphism in the Sierra Albarrana area (Variscan Belt, Iberian Massif), *Journal of Petrology*, *38*, 35-64.

Azor, A., F. G. Lodeiro, and J. F. Simancas (1994), Tectonic evolution of the boundary between the Central Iberian and Ossa-Morena zones (Variscan belt, southwest Spain), *Tectonics*, *13*, 45-61.

Azor, A., F. González Lodeiro, A. Marcos, and J. F. Simancas (1991), Edad y estructura de las rocas de Sierra Albarrana (SW del Macizo Hespérico). Implicaciones regionales, *Geogaceta*, *10*, 119-124.

Azor, A., D. Rubatto, J. F. Simancas, F. González Lodeiro, D. Martínez Poyatos, L. M. Martín Parra, and J. Matas (2008), Rheic Ocean ophiolitic remnants in southern Iberia questioned by SHRIMP U-Pb zircon ages on the Beja-Acebuches amphibolites, *Tectonics*, *27*, TC5006.

Berthé, D., P. Choukroune, and P. Jegouzo (1979), Orthogneiss, mylonite and non coaxial deformation of granites: the example of the South Armorican Shear Zone, *Journal of Structural Geology*, *1*, 31-42.

Braun, J. (1993), Three- dimensional numerical modeling of compressional orogenies: Thrust geometry and oblique convergence, *Geology*, *21*, 153-156.

Brueckner, H. K., H. G. Avé Lallemant, V. B. Sisson, G. E. Harlow, S. R. Hemming, U. Martens, T. Tsujimori, and S. S. Sorensen (2009), Metamorphic reworking of a high pressure–low temperature mélange along the Motagua fault, Guatemala: A record of Neocomian and Maastrichtian transpressional tectonics, *Earth and Planetary Science Letters*, *284*(1), 228-235.

Burg, J. P., M. Iglesias, P. Laurent, P. Matte, and A. Ribeiro (1981), Variscan intracontinental deformation: the Coimbra-Cordoba shear zone (SW Iberian Peninsula), *Tectonophysics*, *78*, 161-177.

Cardozo, N., and R. W. Allmendinger (2013), Spherical projections with OSXStereonet, *Computers & Geosciences*, *51*(0), 193 - 205.

Casas, A. M., D. Gapais, T. Nalpas, K. Besnard, and T. Román- Berdiel (2001), Analogue models of transpressive systems, *Journal of Structural Geology*, *23*, 733- 743.

Cocks, L. R. M., and T. H. Torsvik (2002), Earth geography from 500 to 400 million years ago: a faunal and palaeomagnetic review, *Journal of the Geological Society*, *159*, 631-644.

Chacon, J., M. Delgado-Quesada, and A. Garrote (1974), Sobre la existencia de dos diferentes dominios de metamorfismo regional en la banda Elvas-Badajoz-Córdoba (Macizo Hespérico Meridional), *Boletín Geologico y Minero*, *86*, 61-65.

Chacón, J. (1979), Estudio geológico del sector central del anticlinorio Portoalegre-Badajoz-Córdoba. (Macizo Ibérico Meridional), PhD thesis, 728 pp, Universidad de Granada.

Chacón, J. (1982), El límite entre las Zonas Centro-Iberica y Ossa Morena al Este de la Tierra de Barros (SW del Macizo Ibérico, Badajoz), *Cuadernos do Laboratorio Xeolóxico de Laxe*, *3*, 163-182.

Chichorro, M. (2006), Tectonic evolution of Montemor-o-Novo Shear Zone (SW Ossa Morena Zone - Santiago do Escoural - Cabrela Área), Ph.D. thesis, 569 pp, Universidade de Évora, Évora, Portugal.

Delgado Quesada, M. (1971), Esquema Geológico de la hoja No. 878 de Azuaga (Badajoz), *Boletín Geológico Minero*, *82*, 277-286.

Dewey, J. F. (1977), Suture zone complexities - Review, *Tectonophysics*, *40*, 53-67.

Dewey, J. F., R. E. Holdsworth, and R. A. Strachan (1998), Transpression and transtension zones, in *Continental Transpressional and Transtensional Tectonics*, edited by R. E. Holdsworth, R. A. Strachan and J. F. Dewey, pp. 1-14, Geological Society, London, Special Publications.

Díaz-Azpiroz, M., L. Barcos, J. C. Balanyá, C. Fernández, I. Expósito, and D. M. Czeck (2014), Applying a general triclinic transpression model to highly partitioned brittle-ductile shear zones: A case study from the Torcal de Antequera massif, external Betics, southern Spain, *Journal of Structural Geology*, *68*, 316-336.

Díez Fernández, R., and R. Arenas (2015), The Late Devonian Variscan suture of the Iberian Massif: A correlation of high-pressure belts in NW and SW Iberia, *Tectonophysics*, *654*, 96-100.

Díez Fernández, R., and M. F. Pereira (2017), Strike-slip shear zones of the Iberian Massif: are they coeval?, *Lithosphere*, *9*(5), 726-744.

Díez Fernández, R., J. R. Martínez Catalán, R. Arenas, and J. Abati (2011), Tectonic evolution of a continental subduction-exhumation channel: Variscan structure of the basal allochthonous units in NW Spain, *Tectonics*, *30*, TC3009.

Díez Fernández, R., J. R. Martínez Catalán, R. Arenas, and J. Abati (2012), The onset of the assembly of Pangaea in NW Iberia: Constraints on the kinematics of continental subduction, *Gondwana Research*, *22*, 20-25.

Díez Fernández, R., A. Jiménez-Díaz, R. Arenas, M. F. Pereira, and J. Fernández-Suárez (2019), Ediacaran Obduction of a Fore-arc Ophiolite in SW Iberia: A Turning Point in the Evolving Geodynamic Setting of Peri-Gondwana, *Tectonics*, *38*, 95-119.

Díez Fernández, R., R. Arenas, E. Rojo-Pérez, S. Sánchez Martínez, and J. M. Fuenlabrada (2021), Tectonostratigraphy of the Mérida Massif reveals a new Cadomian suture zone exposure in Gondwana (SW Iberia), *International Geology Review*, doi: 10.1080/00206814.2020.1858355.

Díez Fernández, R., J. M. Fuenlabrada, M. Chichorro, M. F. Pereira, S. Sánchez Martínez, J. B. Silva, and R. Arenas (2017), Geochemistry and tectonostratigraphy of the basal allochthonous units of SW Iberia (Évora Massif, Portugal): keys to the reconstruction of pre-Pangean paleogeography in southern Europe, *Lithos*, *268-271*, 285-301.

Díez Fernández, R., J. Matas, R. Arenas, L. M. Martín-Parra, S. Sánchez Martínez, I. Novo-Fernández, and E. Rojo-Pérez (in press), Two-step obduction of the Porvenir Serpentinite: a cryptic Devonian suture in SW Iberian Massif (Ossa-Morena Complex), in *Special Paper in honor of Eldridge M. Moores*, edited by J. Wakabayashi, Y. Dilek and Y. Ogawa, GSA Books.

Díez Fernández, R., R. Arenas, M. F. Pereira, S. Sánchez Martínez, R. Albert, L. M. Martín Parra, F. J. Rubio Pascual, and J. Matas (2016), Tectonic evolution of Variscan Iberia: Gondwana - Laurussia collision revisited, *Earth-Science Reviews*, *162*, 269-292.

Díez Fernández, R., C. Fernández, R. Arenas, I. Novo-Fernández (2021), Structural data from the Azuaga Fault zone (SW Iberia), *Mendeley Data*, V1, doi: 10.17632/6fvv5t892x.1.

Eguiluz, L., B. Ábalos, and R. Ramón-Lluch (1990), El cabalgamiento de Monesterio (Zona de Ossa-Morena). Microestructuras e implicaciones geodinámicas, *Cuadernos do Laboratorio Xeolóxico de Laxe*, *15*, 61-78.

Eguíluz, L., J. I. Gil Ibarguchi, B. Abalos, and A. Apraiz (2000), Superposed Hercynian and Cadomian orogenic cycles in the Ossa-Morena zone and related areas of the Iberian Massif, *Geological Society of America Bulletin*, *112*, 1398-1413.

Escuder Viruete, J. E., R. Arenas, and J. R. Martínez Catalán (1994), Tectonothermal evolution associated with Variscan crustal extension in the Tormes gneiss dome (NW Salamanca, Iberian massif, Spain), *Tectonophysics*, *238*, 117-138.

Expósito, I., J. F. Simancas, F. González Lodeiro, A. Azor, and D. J. Martínez Poyatos (2002), La estructura de la mitad septentrional de la Zona de Ossa-Morena: deformación en el bloque inferior de un cabalgamiento cortical de evolución compleja, *Revista de la Sociedad Geológica de España*, *15*, 3-14.

Expósito Ramos, I. (2005), Evolución estructural de la mitad septentrional de la Zona de Ossa-Morena y su relación con el límite Zona Ossa-Morena/Zona Centroibérica, *Nova Terra*, *27*, 1-286.

Faure, M., J.-M. Lardeaux, and P. Ledru (2009), A review of the pre-Permian geology of the Variscan French Massif Central, *Comptes Rendus Geoscience*, *341*, 202-213.

Faure, M., E. Bé Mézème, A. Cocherie, P. Rossi, A. Chemenda, and D. Boutelier (2008), Devonian geodynamic evolution of the Variscan Belt, insights from the French Massif Central and Massif Armoricain, *Tectonics*, *27*, TC2005.

Fernández-Suárez, J., G. Gutierrez-Alonso, S. T. Johnston, T. E. Jeffries, D. Pastor-Galán, G. A. Jenner, and J. B. Murphy (2011), Iberian late-Variscan granitoids: Some considerations on crustal sources and the significance of "mantle extraction ages", *Lithos*, *123*(1), 121-132.

Fernández, C., and M. Díaz-Azpiroz (2009), Triclinic transpression zones with inclined extrusion, *Journal of Structural Geology*, *31*, 1255-1269.

Fernández, C., D. M. Czeck, and M. Díaz-Azpiroz (2013), Testing the model of oblique transpression with oblique extrusion in two natural cases: Steps and consequences, *Journal of Structural Geology*, *54*, 85-102.

Fossen, H., and B. Tikoff (1993), The deformation matrix for simultaneous simple shearing, pure shearing and volume change, and its application to transpression transtension tectonics, *Journal of Structural Geology*, *15*, 413-422.

Fossen, H., and B. Tikoff (1997), Forward modeling of non-steady-state deformations and the `minimum strain path', *Journal of Structural Geology*, *19*, 987-996.

Fossen, H., and B. Tikoff (1998), Extended models of transpression and transtension, and application to tectonic settings, *Continental Transpressional and Transtensional Tectonics*, 15-33.

Fossen, H., C. Teyssier, and D. L. Whitney (2013), Transtensional folding, *Journal of Structural Geology*, *56*, 89-102.

Franke, W. (2000), The mid-European segment of the Variscides: Tectonostratigraphic units, terrane boundaries and plate tectonic evolution, in *Orogenic Processes: Quantification and Modelling in the Variscan Belt*, edited by W. Franke, V. Haak, O. Oncken and D. Tanner, pp. 35-61, doi: 10.1144/GSL.SP.2000.1179.1101.1105, Geological Society, London, Special Publications.

Franke, W., L. R. M. Cocks, and T. H. Torsvik (2017), The Palaeozoic Variscan oceans revisited, *Gondwana Research*, *48*, 257-284.

Gabaldón, V., A. Garrote, and C. Quesada (1985), El Carbonífero Inferior del Norte de la Zona de Ossa-Morena (SW de España), *CR 10th International Carboniferous Congress, Madrid*, *3*, 173-186.

García Casquero, J. L., H. N. A. Priem, N. A. I. M. Boelrijk, and J. Chacon (1988), Isotopic dating of the mylonitization of the Azuaga Group in the Badajóz-Córdoba belt, SW Spain, *Geologische Rundschau*, *77*, 483-489.

Garrote, A. (1976), Asociaciones minerales del núcleo metamórfico de Sierra Albarrana (Prov. de Córdoba), *Memórias e notícas. Publicações do Museu e Laboratório Mineralógico e Geológico da Universidade de Coimbra*, *82*, 17-40.

Gómez Barreiro, J., J. R. Martínez Catalán, D. Prior, H.-R. Wenk, S. Vogel, F. Díaz García, R. Arenas, S. Sánchez Martínez, and I. Lonardelli (2010), Fabric Development in a Middle Devonian Intraoceanic Subduction Regime: The Careón Ophiolite (Northwest Spain), *The Journal of Geology*, *118*, 163-186.

González del Tánago, J. (1995), El núcleo metamórfico de Sierra Albarrana y su campo de pegmatitas graníticas asociado, Macizo Ibérico, Córdoba, *Nova Terra*, *12*, 1-713.

González del Tánago, J., and R. Arenas (1991), Anfibolitas granatíferas de Sierra Albarrana, Córdoba : termobarometría e implicaciones para el desarrollo del metamorfismo regional, *Revista de la Sociedad Geológica de España*, *4*, 251-269.

Guillot, S. p., S. di Paola, R.-P. Ménot, P. Ledru, M. I. Spalla, G. Gosso, and S. p. Schwartz (2009), Suture zones and importance of strike-slip faulting for Variscan geodynamic reconstructions of the External Crystalline Massifs of the western Alps, *Bulletin de la Société Géologique de France*, *180*(6), 483-500.

Hartung, W. (1941), Pflanzenreste aus dem südspanischen Karbon (Nordrand der Provinz Sevilla), *Jahrbuch der Reichsstelle für Bodenforschung für 1940*, *61*, 267-277.

Hatcher, R. D. (1978), Tectonics of the western Piedmont and Blue Ridge, southern Appalachians: Review and Speculation, *American Journal of Science*, *278*, 276-304.

Hirn, A., A. Nercessian, M. Sapin, G. Jobert, X. Z. Xin, G. E. Yuan, L. D. Yuan, and T. J. Wen (1984), Lhasa block and bordering sutures— a continuation of a 500-km Moho traverse through Tibet, *Nature*, *307*(5946), 25-27.

Hodges, K. V. (2000), Tectonics of the Himalaya and southern Tibet from two perspectives, *Geological Society of America Bulletin*, *112*, 324-350.

Hutton, D. H. W. (2009), Strike-slip terranes and a model for the evolution of the British and Irish Caledonides, *Geological Magazine*, *124*(5), 405-425.

Iglesias Ponce de Leon, M., and P. Choukroune (1980), Shear zones in the Iberian arc, *Journal of Structural Geology*, *2*, 63-68.

Jackson, P., and D. J. Sanderson (1992), Scaling of fault displacements from the Badajoz-Cordoba shear zone, SW Spain, *Tectonophysics*, *210*, 179-190.

Jensen, S., T. Palacios, and L. Eguiluz (2004), Cambrian ichnofabrics from the Ossa Morena and Central Iberian zones: preliminary results, *Geo-Temas*, *6*(2), 291-293.

Jiang, D., S. Lin, and P. F. Williams (2001), Deformation path in high-strain zones, with reference to slip partitioning in transpressional plate-boundary regions, *Journal of Structural Geology*, *23*, 991-1005.

Jones, R. R., R. E. Holdsworth, P. Clegg, K. McCaffrey, and E. Tavarnelli (2004), Inclined transpression, *Journal of Structural Geology*, *26*, 1531-1548.

Julivert, M., Fontboté, J.M., Ribeiro, A., Nabais-Conde, L.E. (1972), Mapa tectónico de la Península Ibérica y Baleares a escala 1:1.000.000. *IGME, Memoria explicativa*, 1-113.

Kroner, U., and R. L. Romer (2013), Two plates — Many subduction zones: The Variscan orogeny reconsidered, *Gondwana Research*, *24*, 298-329.

Leever, K. A., R. H. Gabrielsen, D. Sokoutis, and E. Willingshofer (2011), The effect of convergence angle on the kinematic evolution of strain partitioning in transpressional brittle wedges: Insight from analog modeling and high-resolution digital image analysis, *Tectonics*, *30*, TC2013.

Lin, S. F., D. Jiang, and P. F. Williams (1998), Transpression (or transtension) zones of triclinic symmetry: natural example and theoretical modelling, *Continental Transpressional and Transtensional Tectonics*, 41-57.

Liñán, E. (1978), Bioestratigrafía de la Sierra de Córdoba, PhD thesis, 212 pp, Universidad de Granada, Granada.

López Sánchez-Vizcaíno, V., M. T. Gómez-Pugnaire, A. Azor, and J. M. Fernández-Soler (2003), Phase diagram sections applied to amphibolites: a case study from

the Ossa-Morena/Central Iberian Variscan suture (Southwestern Iberian Massif), *Lithos*, *68*(1), 1-21.

Lotze, F. (1945), Zur Gliederung der Varisziden der Iberischen Meseta. *Geotektonische Forschungen, 6*, 78-92

Llana-Fúnez, S., and A. Marcos (2001), The Malpica-Lamego Line: a major crustal-scale shear zone in the Variscan belt of Iberia, *Journal of Structural Geology*, *23*, 1015-1030.

Marcos, A., A. Azor, F. González Lodeiro, and F. Simancas (1991), Early phanerozoic trace fossils from the Sierra Albarrana Quartzites (Ossa-Morena Zone, Southwest Spain), *Scripta Geologica*, *97*, 47-53.

Martínez Catalán, J. R., S. Collett, K. Schulmann, P. Aleksandrowski, and S. Mazur (2020), Correlation of allochthonous terranes and major tectonostratigraphic domains between NW Iberia and the Bohemian Massif, European Variscan belt, *International Journal of Earth Sciences*, *109*(4), 1105-1131.

Martínez Catalán, J. R., R. Arenas, F. Díaz García, F. J. Rubio Pascual, J. Abati, and J. Marquínez García (1996), Variscan exhumation of a subducted paleozoic continental margin: The basal units of the Ordenes Complex, Galicia, NW Spain, *Tectonics*, *15*, 106-121.

Martínez Catalán, J. R., F. Díaz García, R. Arenas, J. Abati, P. Castiñeiras, P. González Cuadra, J. Gómez Barreiro, and F. J. Rubio Pascual (2002), Thrust and detachment systems in the Ordenes Complex (northwestern Spain): Implications for the Variscan-Appalachian geodynamics, in *Variscan-Appalachian Dynamics: The Building of the Late Paleozoic Basement*, edited by J. R. Martínez Catalán, R. D. Hatcher, R. Arenas and F. Díaz García, pp. 163-182,

doi: 110.1130/1130-8137-2364-1137.1163, Geological Society of America Special Paper.

Martínez Catalán, J. R., et al. (2009), A rootless suture and the loss of the roots of a mountain chain: The Variscan belt of NW Iberia, *Comptes Rendus Geoscience*, *341*, 114-126.

Martínez Poyatos, D., J. F. Simancas, A. Azor, and F. González Lodeiro (1995), La estructura del borde meridional de la Zona Centroibérica en el sector suroriental de la Provincia de Badajoz, *Revista de la Sociedad Geológica de España*, *8*, 41-50.

Martínez Poyatos, D., J. F. Simancas, A. Azor, and F. González Lodeiro (1998a), La estructura del borde meridional de la Zona Centroibérica (Macizo Ibérico) en el Norte de la Provincia de Córdoba, *Revista de la Sociedad Geológica de España*, *11*, 87-94.

Martínez Poyatos, D., J. F. Simancas, A. Azor, and F. González Lodeiro (1998b), Evolution of a Carboniferous piggyback basin in the southern Central Iberian Zone (Variscan Belt, SE Spain), *Bulletin de la Société Geologique de France*, *169*, 573-578.

Martínez Poyatos, D., F. Nieto, A. Azor, and J. F. Simancas (2001), Relationships between very low-grade metamorphism and tectonic deformation: examples from the southern Central Iberian Zone (Iberian Massif, Variscan Belt), *Journal of the Geological Society*, *158*, 953-968.

Martínez Poyatos, D. J. (2002), Estructura del borde meridional de la Zona Centroibérica y su relación con el contacto entre las Zonas Centroibérica y de Ossa-Morena, *Nova Terra*, *18*, 1-295.

Matte, P. (1986), Tectonics and plate tectonics model for the Variscan belt of Europe, *Tectonophysics*, *126*, 329-374.

Matte, P. (1991), Accretionary history and crustal evolution of the Variscan belt in Western Europe, *Tectonophysics*, *196*, 309-337.

Matte, P. (2001), The Variscan collage and orogeny (480-290 Ma) and the tectonic definition of the Armorica microplate: a review, *Terra Nova*, *13*, 122-128.

McCaffrey, K., P. C. Zwick, Y. Bock, L. Prawirodirdjo, J. F. Genrich, C. W. Stevens, S. S. O. Puntodewo, and C. Subarya (2000), Strain partitioning during oblique plate convergence in northern Sumatra: Geodetic and seismologic constraints and numerical modeling, *Journal of Geophysical Research*, *105*, 28363-28376.

McClay, K. R., P. S. Whitehouse, T. Dooley, and M. Richards (2004), 3D evolution of fold and thrust belts formed by oblique convergence, *Marine and Petroleum Geology*, *21*, 857- 877.

Means, W. D. (1989), Stretching faults, *Geology*, *17*, 893-896.

Moita, P., J. Munhá, P. E. Fonseca, J. Pedro, C. C. G. Tassinari, A. Araújo, and T. Palacios (2005), Phase equilibria and geochronology of Ossa-Morena eclogites, paper presented at XIV Semana de Geoquímica, VIII Congresso de Geoquímica dos Paises de Lingua Portuguese, 2005.

Murphy, J. B., C. Quesada, G. Gutiérrez-Alonso, S. T. Johnston, and A. Weil (2016), Reconciling competing models for the tectono-stratigraphic zonation of the Variscan orogen in Western Europe, *Tectonophysics*, *681*, 209-219.

Nabavi, S. T., S. A. Alavi, M. Díaz-Azpiroz, S. Mohammadi, M. R. Ghassemi, C. Fernández, L. Barcos, and M. Frehner (2020), Deformation mechanics in inclined, brittle-ductile transpression zones: Insights from 3D finite element modelling, *Journal of Structural Geology*, *137*.

Oyhantçabal, P., S. Siegesmund, K. Wemmer, and C. W. Passchier (2011), The transpressional connection between Dom Feliciano and Kaoko Belts at 580–550 Ma, *International Journal of Earth Sciences*, *100*(2), 379-390.

Passchier, C. W. (1997), The fabric attractor, *Journal of Structural Geology*, *19*, 113-127.

Pereira, M. F., A. Apraiz, J. B. Silva, and M. Chichorro (2008), Tectonothermal analysis of high-temperature mylonitization in the Coimbra-Cordoba shear zone (SW Iberian Massif, Ouguela tectonic unit, Portugal): Evidence of intra-continental transcurrent transport during the amalgamation of Pangea, *Tectonophysics*, *461*, 378-394.

Pereira, M. F., A. Apraiz, M. Chichorro, J. B. Silva, and R. A. Armstrong (2010a), Exhumation of high-pressure rocks in northern Gondwana during the Early Carboniferours (Coimbra-Cordoba shear zone, SW Iberian Massif): Tectonothermal analysis and U–Th–Pb SHRIMP in-situ zircon geochronology, *Gondwana Research*, *17*, 440-460.

Pereira, M. F., J. B. Silva, K. Drost, M. Chichorro, and A. Apraiz (2010b), Relative timing of transcurrent displacements in northern Gondwana: U–Pb laser ablation ICP-MS zircon and monazite geochronology of gneisses and sheared granites from the western Iberian Massif (Portugal), *Gondwana Research*, *17*, 461-481.

Pereira, M. F., M. Chichorro, I. S. Williams, J. B. Silva, C. Fernández, M. Díaz-Azpíroz, A. Apraiz, and A. Castro (2009), Variscan intra-orogenic extensional tectonics in the Ossa-Morena Zone (Évora-Aracena-Lora del Río metamorphic belt, SW Iberian Massif): SHRIMP zircon U–Th–Pb geochronology, *Geological Society, London, Special Publications*, *327*, 215-237.

Pérez-Cáceres, I., D. Martínez Poyatos, J. F. Simancas, and A. Azor (2015), The elusive nature of the Rheic Ocean suture in SW Iberia, *Tectonics*, *34*(12), 2429-2450.

Pérez-Cáceres, I., J. F. Simancas, D. Martínez Poyatos, A. Azor, and F. González Lodeiro (2016), Oblique collision and deformation partitioning in the SW Iberian Variscides, *Solid Earth*, *7*, 857-872.

Philippon, M., and G. Corti (2016), Obliquity along plate boundaries, Tectonophysics, 693, 171-182.

Platt, J. P. (1986), Dynamics of orogenic wedges and the uplift of high-pressure metamorphic rocks, *Geological Society of America Bulletin*, *97*, 1037-1053.

Quesada, C. (1990), Precambrian successions in SW Iberia: their relationship to 'Cadomian' orogenic events, in *The Cadomian Orogeny*, edited by D. R. Lemos, R. A. Strachan and C. G. Topley, pp. 353-362, Geological Society, London, Special Publication.

Quesada, C., and R. D. Dallmeyer (1994), Tectonothermal evolution of the Badajoz-Cordoba shear zone (SW Iberia): characteristics and $^{40}Ar/^{39}Ar$ mineral age constraints, *Tectonophysics*, *231*, 195-213.

Ramsay, J. G., and R. H. Graham (1970), Strain variation in shear belts, *Canadian Journal of Earth Sciences*, *7*, 786-813.

Richard, P., and P. R. Cobbold (1990), Experimental insights into partitioning of fault motions in continental convergent wrench zones, *Annales Tectonicae*, *4*, 35- 44.

Robardet, M., and J. C. Gutiérrez Marco (2004), The Ordovician, Silurian and Devonian sedimentary rocks of the Ossa-Morena Zone (SW Iberian Peninsula, Spain), *Journal of Iberian Geology*, *30*, 73-92.

Rojo-Pérez, E., R. Arenas, J. M. Fuenlabrada, S. Sánchez Martínez, L. M. Martín Parra, J. Matas, A. P. Pieren, and R. Díez Fernández (2019), Contrasting isotopic

sources (Sm-Nd) of Late Ediacaran series in the Iberian Massif: Implications for the Central Iberian-Ossa Morena boundary, *Precambrian Research*, *324*, 194-207.

Rosas, F. M., F. O. Marques, M. Ballèvre, and C. Tassinari (2008), Geodynamic evolution of the SW Variscides: Orogenic collapse shown by new tectonometamorphic and isotopic data from western Ossa-Morena Zone, SW Iberia, *Tectonics*, *27*, doi: 10.1029/2008TC002333.

San José, M. A., P. Herranz, and A. P. Pieren (2004), A review of the Ossa-Morena Zone and its limits. Implications for the definition of the Lusitan-Marianic Zone, *Journal of Iberian Geology*, *30*, 7-22.

Sánchez-García, T., F. Bellido, and C. Quesada (2003), Geodynamic setting and geochemical signatures of Cambrian–Ordovician rift-related igneous rocks (Ossa-Morena Zone, SW Iberia), *Tectonophysics*, *365*, 233-255.

Schulmann, K., A. B. Thompson, O. Lexa, and J. Jezek (2003), Strain distribution and fabric development modeled in active and acient transpressive zones, *Journal of Geophysical Research*, *108*.

Schulmann, K., O. Lexa, V. Janoušek, J. M. Lardeaux, and J. B. Edel (2014), Anatomy of a diffuse cryptic suture zone: An example from the Bohemian Massif, European Variscides, *Geology*, *42*(4), 275-278.

Shaw, J., and S. T. Johnston (2016), Oroclinal buckling of the Armorican ribbon continent: An alternative tectonic model for Pangean amalgamation and Variscan orogenesis, *Lithosphere*, *8*(6), 769-777.

Simancas, J. F., A. Tahiri, A. Azor, F. González Lodeiro, D. J. Martínez Poyatos, and H. E. Hadi (2005), The tectonic frame of the Variscan–Alleghanian orogen in Southern Europe and Northern Africa, *Tectonophysics*, *398*, 181-198.

Simancas, J. F., P. Ayarza, A. Azor, R. Carbonell, D. Martínez Poyatos, A. Pérez-Estaún, and F. González Lodeiro (2013), A seismic geotraverse across the Iberian Variscides: Orogenic shortening, collisional magmatism, and orocline development, *Tectonics*, *32*, 417-432.

Simancas, J. F., et al. (2003), Crustal structure of the transpressional Variscan orogen of SW Iberia: SW Iberia deep seismic reflection profile (IBERSEIS), *Tectonics*, *22*, 1062.

Solá, A. R., I. S. Williams, A. M. R. Neiva, and M. L. Ribeiro (2009), U–Th–Pb SHRIMP ages and oxygen isotope composition of zircon from two contrasting late Variscan granitoids, Nisa-Albuquerque batholith, SW Iberian Massif: Petrologic and regional implications, *Lithos*, *111*, 156-167.

Stampfli, G. M., C. Hochard, C. Vérard, C. Wilhem, and J. vonRaumer (2013), The formation of Pangea, *Tectonophysics*, *593*, 1-19.

Sullivan, W. A., and R. D. Law (2007), Deformation path partitioning within the transpressional White Mountain shear zone, California and Nevada, *Journal of Structural Geology*, *29*(4), 583-599.

Taylor, M., A. Yin, F. J. Ryerson, P. Kapp, and L. Ding (2003), Conjugate strike-slip faulting along the Bangong-Nujiang suture zone accommodates coeval east-west extension and north-south shortening in the interior of the Tibetan Plateau, *Tectonics*, *22*(4).

Tikoff, B., and H. Fossen (1995), The limitations of three-dimensional kinematic vorticity analysis, *Journal of Structural Geology*, *17*, 1771-1784.

Torvela, T., and C. Ehlers (2010), From ductile to brittle deformation: structural development and strain distribution along a crustal-scale shear zone in SW Finland, *International Journal of Earth Sciences*, *99*(5), 1133-1152.

Truesdell, C. A. (1953), Two measures of vorticity, *Journal of Rational Mechanical Analysis*, *2*, 173-217.

Vanderhaeghe, O. (2012), The thermal-mechanical evolution of crustal orogenic belts at convergent plate boundaries: a reappraisal of the orogenic cycle, *Journal of Geodynamics*, *56-57*, 124-145.

Vernant, P., and J. Chéry (2006), Mechanical modelling of oblique convergence in the Zagros, Iran, *Geophysical Journal International*, *165*, 991-1002.

Wallis, S. (1998), Exhuming the Sanbagawa metamorphic belt: the importance of tectonic discontinuities, *Journal of Metamorphic Geology*, 16, 83-95.

Weil, A. B., G. Gutiérrez-Alonso, S. T. Johnston, and D. Pastor-Galán (2013), Kinematic constraints on buckling a lithospheric-scale orocline along the northern margin of Gondwana: A geologic synthesis, *Tectonophysics*, *582*, 25-49.

Wintsch, R.P., Byrne, T., and M. Toriumi (1999), Exhumation of the Sanbagawa blueschist belt, SW Japan, by lateral flow and extrusion: evidence from structural kinematics and retrograde P-T-t paths, in Exhumation Processes: Normal Faulting, Ductile Flow and Erosion, edited by M.T. Brandon, G.S Lister and S.D. Willett, pp. 129-155, *Geological Society, London, Special Publications*, 154.

Wu, L., J. B. Murphy, C. Quesada, Z. X. Li, J. Waldron, S. Williams, S. Pisarevsky, and W. Collins (2020), The amalgamation of Pangea: Paleomagnetic and geological observations revisited, *Geological Society of America Bulletin*, *10.1130/B35633.1*.

FIGURE CAPTIONS

Figure 1: Sketches showing different relationships between a suture zone and superimposed faults that cut across the suture. Each case is shown within a white box, with a simplified map to the left and a cross-section to the right (white line represents topography). Main foliation and fault traces are oblique to conform to a breaching nature of the faults. Dip angle of the faults is steeper than that of the foliation. In all cases three main lithological ensembles have been recognized. Two lithological ensembles with continental crust affinity bound an exposure of rocks that belong to a suture zone (e.g. high-pressure rocks, ophiolites, etc.). The recognition of upper and lower plate of the suture zone as well as the location of the root zone of the suture depend on the kinematics of the faults that bound the suture zone exposure and on the primary and final geometrical relationships between the suture and those faults. In the simplest case (a), the contacts between lithological ensembles at surface are primary accretionary faults; the exposure of rocks that belong to the suture zone marks its actual root. In the absence of large-scale folds, rocks that belong to the same suture zone should not be exposed to the left or right of this root. (b), (c), (d), and (e) illustrate cases where the contacts (at surface) between lithological ensembles are not accretionary faults but later faults. As in case (a), there should not be additional exposures of rocks that belong to the same suture zone to the left or right. (f), (g), (h), (i) and (j) illustrate cases where the contacts (at surface) are also later faults. In these cases an additional exposure of suture zone rocks is expected to the left. (d), (f), (g), (h) represent cases where the two lithological ensembles that bound the suture zone exposure belong to the same upper (f, g, and h) or lower (d) plate.

Figure 2: Sketch showing the zonation of the Variscan Orogen after *Díez Fernández and Arenas* [2015]. Location of the Iberian Massif (Figure 3) is indicated. Main Variscan

strike-slip shear zones of the Iberian Massif: 1 – Porto-Tomar; 2 – Malpica-Lamego; 3 – Juzbado-Penalva do Castelo; 4 – Douro-Beira; 5 – Huebra; 6 – Tamames; 7 – Palas de Rei; 8 – Coimbra-Córdoba; 9 – South Iberian.

Figure 3: (a) Zonation and major tectonic elements of the Iberian Massif after *Díez Fernández and Arenas* [2015]. Location of the map in Figure 4 is indicated. (b) Inset map and tectonic sketch showing the location of the Coimbra-Córdoba Shear Zone in SW Iberian massif and its general structure in map view. Abbreviations: AF — Azuaga Fault; BToIP — Basal Thrust of the Iberian Parautochthon; BAO — Beja–Acebuches Ophiolite; CA — Carvalhal Amphibolites; CF — Canaleja Fault; CMU — Cubito–Moura Unit; CO — Calzadilla Ophiolite; CU — Central Unit; EsT — Espiel Thrust; EU—Escoural Unit; ET—Espina Thrust; HF— Hornachos Fault; IOMZO —Internal Ossa-Morena Zone Ophiolites; J–PCSZ — Juzbado-Penalva do Castelo Shear Zone; LFT — Lalín-Forcarei Thrust; LPSZ — Los Pedroches Shear Zone; LLSZ — Llanos Shear Zone; MLSZ — Malpica–Lamego Shear Zone; MF — Matachel Fault; OF — Onza Fault; OVD — Obejo–Valsequillo Domain; PG–CVD — Puente Génave–Castelo de Vide Detachment; PRSZ— Palas de Rei Shear Zone; PTSZ — Porto–Tomar Shear Zone; RF — Riás Fault; SISZ — South Iberian Shear Zone; VF — Viveiro Fault; ZSI — Zalamea de la Serena Imbricates.

Figure 4: (a) Geological map of the study area including reference points (e.g. RP-1) referred to in the text (D_3 foliation and lineation are shown in (f)). The location of reference points is indicated by circled numbers. (b), (c), (d) Cross-sections normal to main faults and folds. (e) Stereoplot with structural data from the primary and secondary faults. (f) Geological map showing D_3 fabrics (S_3 and $_mL_3$). Dashed lines demarcate the

domains used for structural analysis in Figure 7. (g) Stereoplot with structural data from brittle (faults) and ductile (S_3 and $_mL_3$) D_3 structures.

Figure 5: (a) Breccias within the fault zone of the Azuaga Fault. Note NE-dipping planes featured by gouges (dashed lines) cutting across the breccias or bounding them. Plane of observation is vertical. (b) SC structures indicating sinistral shearing in phyllonites from the fault zone of the Berlanga-2 Fault. C-planes (white dashed lines) and S-planes (yellow dashed lines) are near-vertical. (c) Slickenlines (red lines) in the fault zone of the Berlanga-1 Fault. (d) Slickenfibres (red lines) in the fault zone of the Azuaga Fault. Note SE-plunging and staircase geometry of the fibres stepping down to the NW (sinistral and reverse dip-slip). (e) SC structures indicating top-to-the-SW tectonic transport in phyllonites and breccias from the fault zone of the Azuaga Fault. C-planes (white dashed lines) and S-planes (yellow dashed lines) show moderate NE-dipping (picture is oblique to the strike of C-planes; actual dip is 55º). (f) Phyllonites after syn-orogenic conglomerates affected by sinistral strike-slip shearing within the fault zone of the Berlanga-2 Fault. Note sigma structure (red dashed lines) of individual clasts. Abbreviations: VOP – Vertical Observation Plane; HOP – Horizontal Observation Plane.

Figure 6: (a) Folded compositional banding (bedding) and main foliation (blue line) in albite-bearing paragneisses of the Central Unit. SW-verging folds are accompanied by crenulation cleavage (S_3). (b) Garnet-bearing amphibolite (retro-eclogite) from the Central Unit. (c) Main foliation (S_2) in alternating paragneisses and felsic orthogneisses deformed into a SW-verging D_3 antiform that occurs close to the Azuaga Fault. The backlimb dips 50º to the NE, while the forelimb is near-vertical. (d) Folded compositional banding and main foliation (white line) in banded phyllites of the Azuaga Formation close

to the Azuaga Fault. Asymmetric parasitic folds are accompanied by crenulation cleavage (S_3; red line) and suggest regional antiform to the NE (i.e., in the Central Unit). (e) Folded bedding in meta-conglomerates of the syn-orogenic strata (white line). Note ellipsoidal shape of individual clasts oriented almost normal to bedding and defining a planar shape fabric (S_3; red line). (f) Rhyolite intruded along the Berlanga-2 Fault. It contains xenoliths of black quartzite (arrow). Abbreviations: VOP – Vertical Observation Plane; HOP – Horizontal Observation Plane.

Figure 7: Stereoplots showing the orientation of bedding (S_0) and main foliation in the Azuaga Formation and Albariza-Bembezar Succession (S_x), and in the Central Unit (S_2). –axes and axial planes are calculated using software Stereonet (*Allmendinger et al.*, 2013; *Cardozo and Allmendinger*, 2013). Data location is indicated in Figure 4f.

Figure 8: (a) Folded main foliation (S_x; blue line) in banded phyllites of the Azuaga Formation. Parasitic folds are accompanied by incipient crenulation cleavage (S_3; red line). (b) Anastomosing rough cleavage (S_3; red) in meta-conglomerates of the Carboniferous syn-orogenics. (c) Compositional banding (bedding; white line) in phyllites and meta-sandstones of the Azuaga Formation deformed into an upright antiform that shows refracted and near-vertical crenulation cleavage (S_3; red line). (d) NE-dipping minor reverse fault featured by breccias and cataclasites (fault zone bounded by white dashed lines). This fault cuts across paired D_3 folds that affect the main foliation in the Azuaga Formation (S_x; blue line). Note the antiform in the hanging wall and the synform in the footwall. Abbreviations: VOP – Vertical Observation Plane; HOP – Horizontal Observation Plane.

Figure 9: Comparison of the structural data from the Azuaga Fault with the predictions of the model of oblique transpression with oblique extrusion (*Fernández and Díaz-Azpiroz*, 2009). (a) Small stereoplot: graph depicting the orientation of the mean shear-zone boundary (szb, orange great circle), its pole (orange triangle), the simple shear direction (orange circle with a pitch of 19.2º SE; angle ϕ), and the range of υ angles (extrusion direction, orange diamonds) considered in this work. Large stereoplot: Example of best-fit between the predictions of the model (orientation of the principal axes *X* and *Z* of the finite strain ellipsoid) for $\upsilon = 50º$ and distinct vorticity (W_k) values. Arrows indicate the reorientation sense of the principal axes of the strain ellipsoid with increasing finite strain. The mean orientations of poles to S_3 (purple circle) and $_mL_3$ (blue circle) are shown together with their respective confidence cones ($\alpha_{95} = 6.0º$ and, 5.6º, respectively). The purple and blue patterns mark the area of concentration of the largest part of poles to S_3 and $_mL_3$ (densities of more than 2% and 10% per 1% area, respectively). (b) Histogram of the angles between $_mL_3$ and the intersection S_3/shear zone boundary. The mean angle is 98º (which is equivalent to 82º), with a confidence angle (α_{95}) of ±5º. (c) Logarithmic deformation diagram depicting the shapes of the strain ellipsoids for distinct deformation sequences taken from selected best-fit results of the kinematic analysis of the Azuaga Fault ($\upsilon = 50º$). (d) Stereoplot with the orientation of the convergence vectors (oblique flow apophysis) for the best-fit results of the kinematic analysis of the Azuaga Fault. The orange pattern shows the azimuth range for the determined convergence vectors. (a and d) Equal-angle, lower-hemisphere projection.

Figure 10: (a), (b), (c) Stereoplots depicting selected, best-fit reorientation paths (*a* to *i*) of fold hinges as passive lines for the three pre-D_3 planar fabrics (S_0, S_x and S_2), compared to the estimated statistical fold axes (blue, red, and purple squares) for the Western (1),

Central-western (2), and Central (3) sections of the Azuaga Fault. For each path the corresponding υ angle, W_k value and original orientation of the folded plane is indicated at the bottom of the figure. (d) Stereoplot showing the statistical results of the pre-D_3 orientation of S_0, S_x and S_2. Mean values and confidence cones (α_{95}) of the poles to those planes are detailed in the table.

Figure 11: Structural model of inclined transpression (based on *Jones et al.*, 2004) with heterogeneous strain adapted to the case study. The Central Unit would occupy a less-strained deformation zone of a sinistral shear zone bounded by dip-slip faults (more strained domains). The D_3 folded structure of Central Unit is the result of late exhumation performed via oblique, upward extrusion from the middle crust of a piece of an underlying Devonian suture zone. S_3 strikes obliquely to the deformation zone and its dip is steeper than the boundaries of the deformation zone. The pitch of D_3 lineation relative to S_3 is moderate to shallow.

Figure 12: Sketches illustrating the late Variscan tectonic evolution of the Central Unit as observed perpendicular to its trace. (a) Hypothesis (ruled out) showing the Central Unit thrust onto the Azuaga Formation before the Carboniferous syn-orogenic strata were deposited (proto-Azuaga Fault). The internal structure of the Central Unit (suture zone) parallels the Azuaga Fault. (b) Same hypothesis as in Figure 12a, although the internal structure of the Central Unit (suture zone) is cut by the Azuaga Fault. The conclusion regarding the continuation of an underlying Devonian suture zone to the SW is similar to that in Figure 12d. (c) Structure inferred for the study area before the Azuaga Fault. (d) Regional structure after the Azuaga Fault. Blue square shows the structure observed in the study area (see Figures 4b, 4c, 4d).

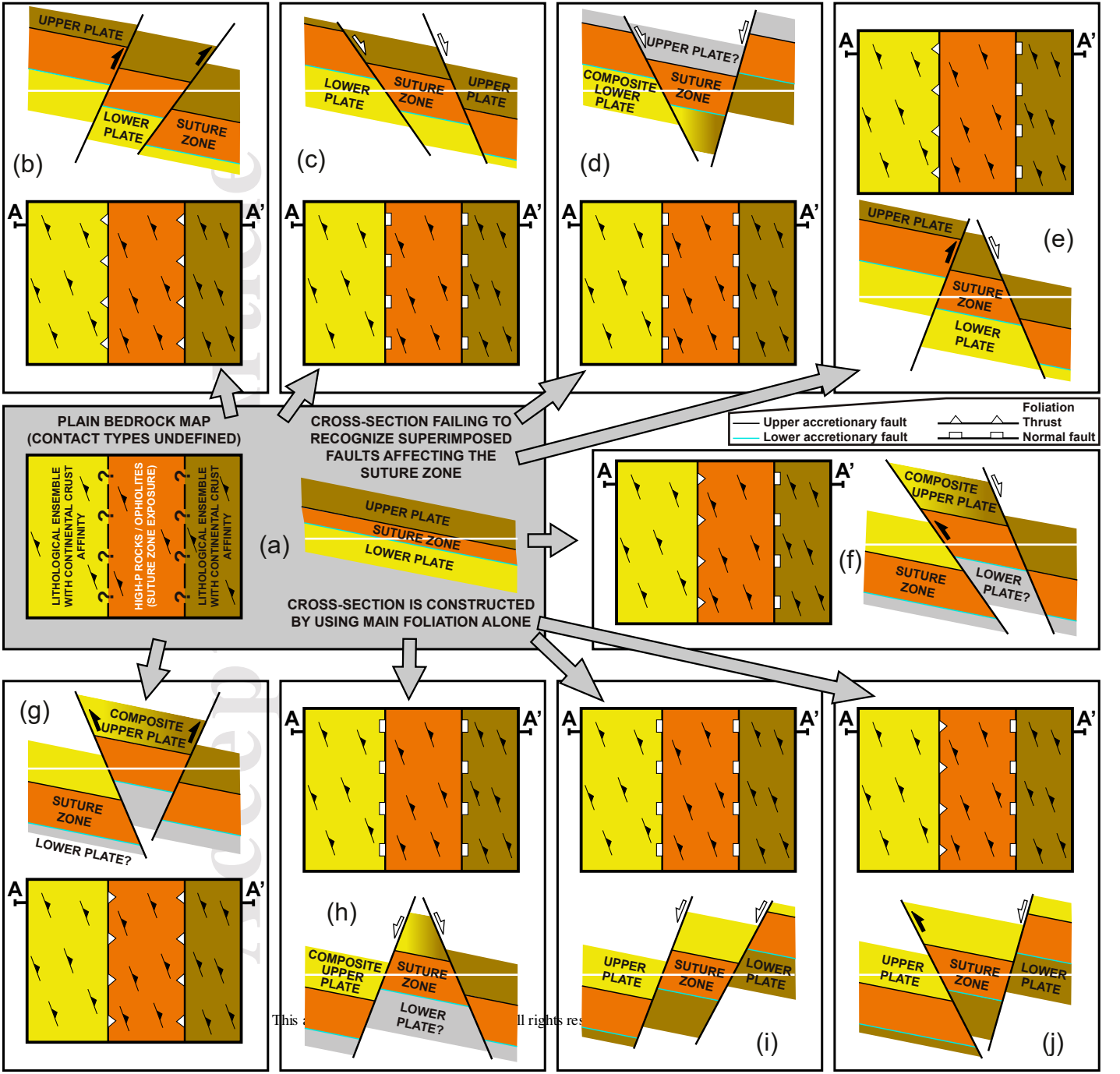

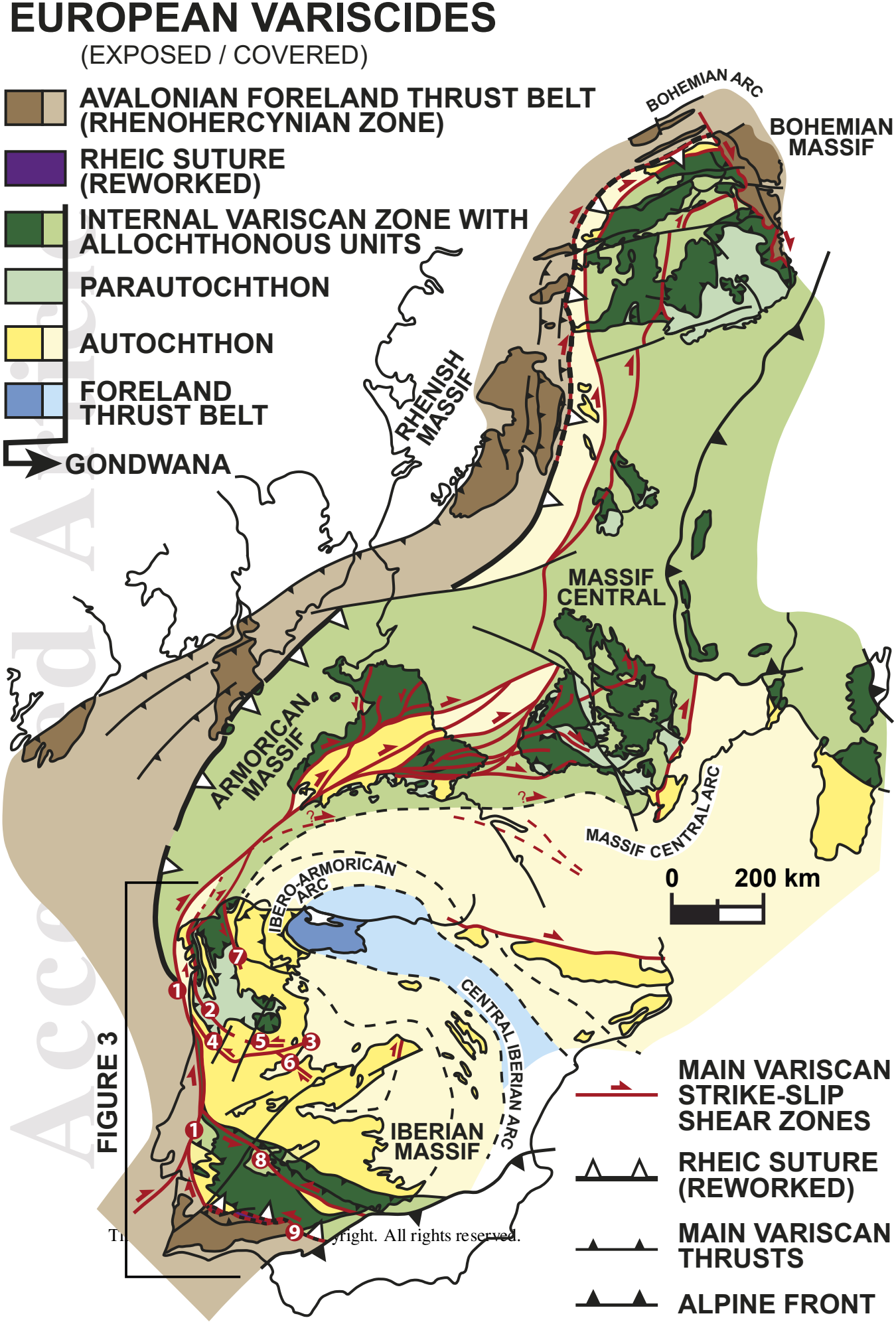

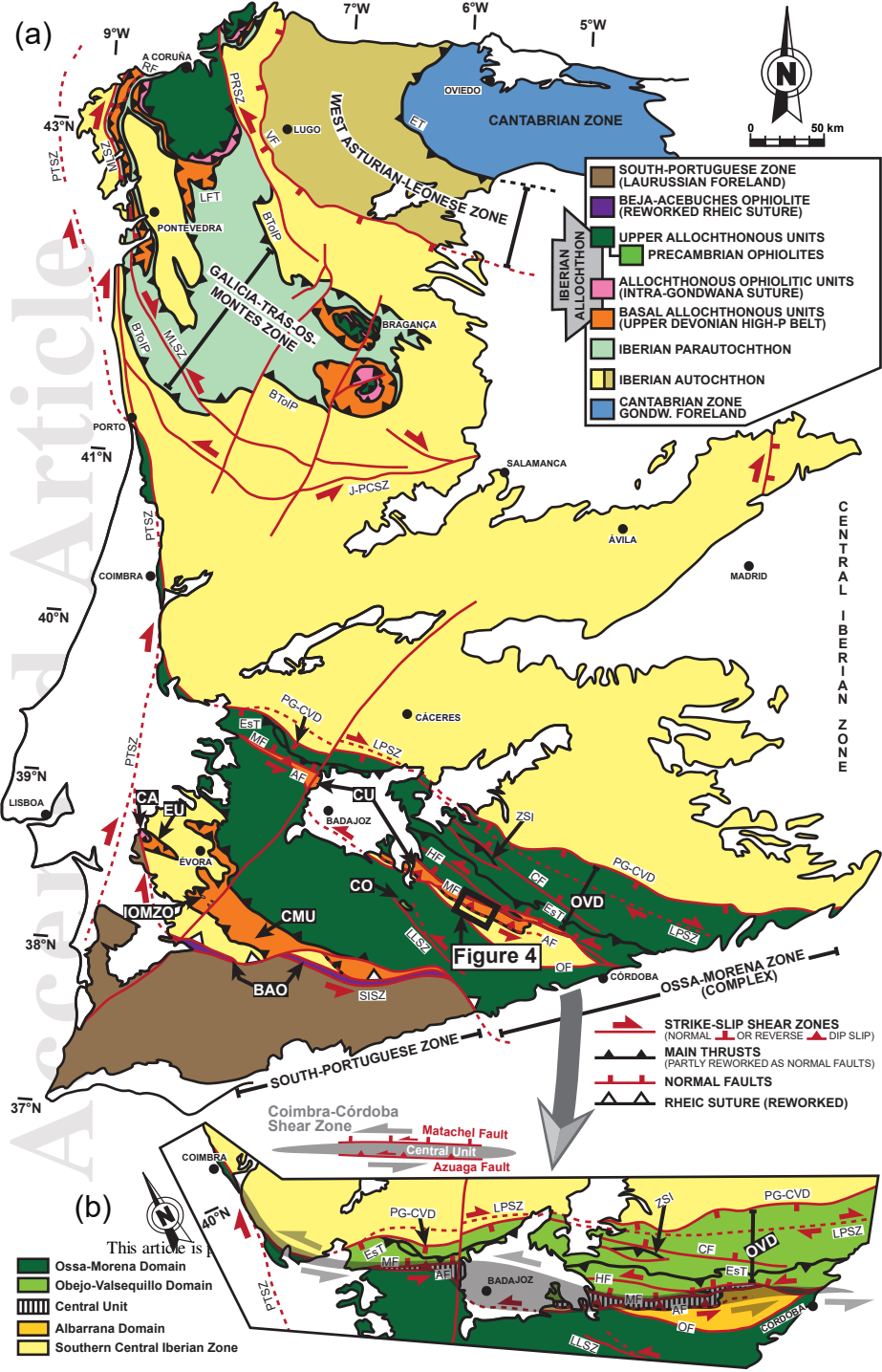

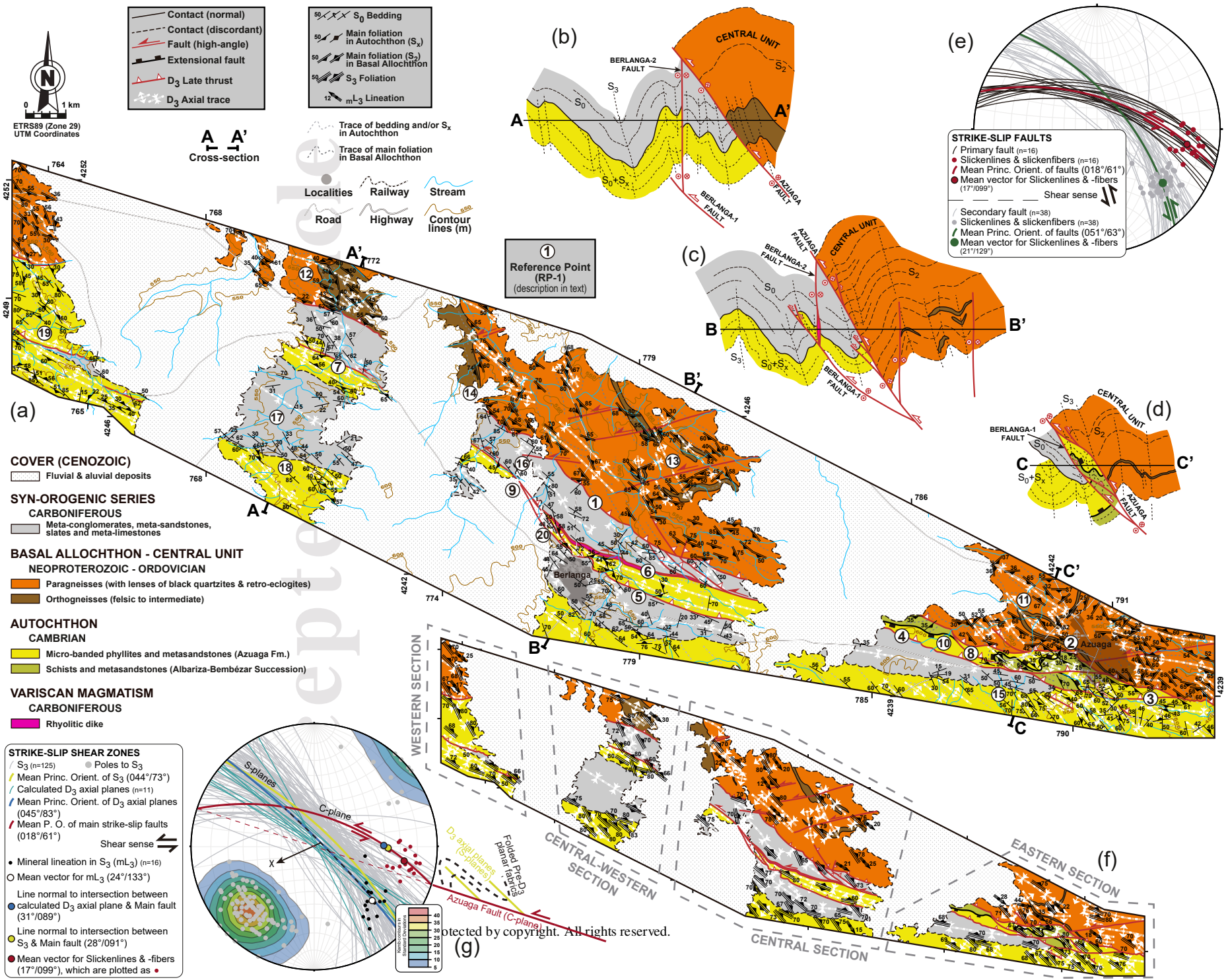

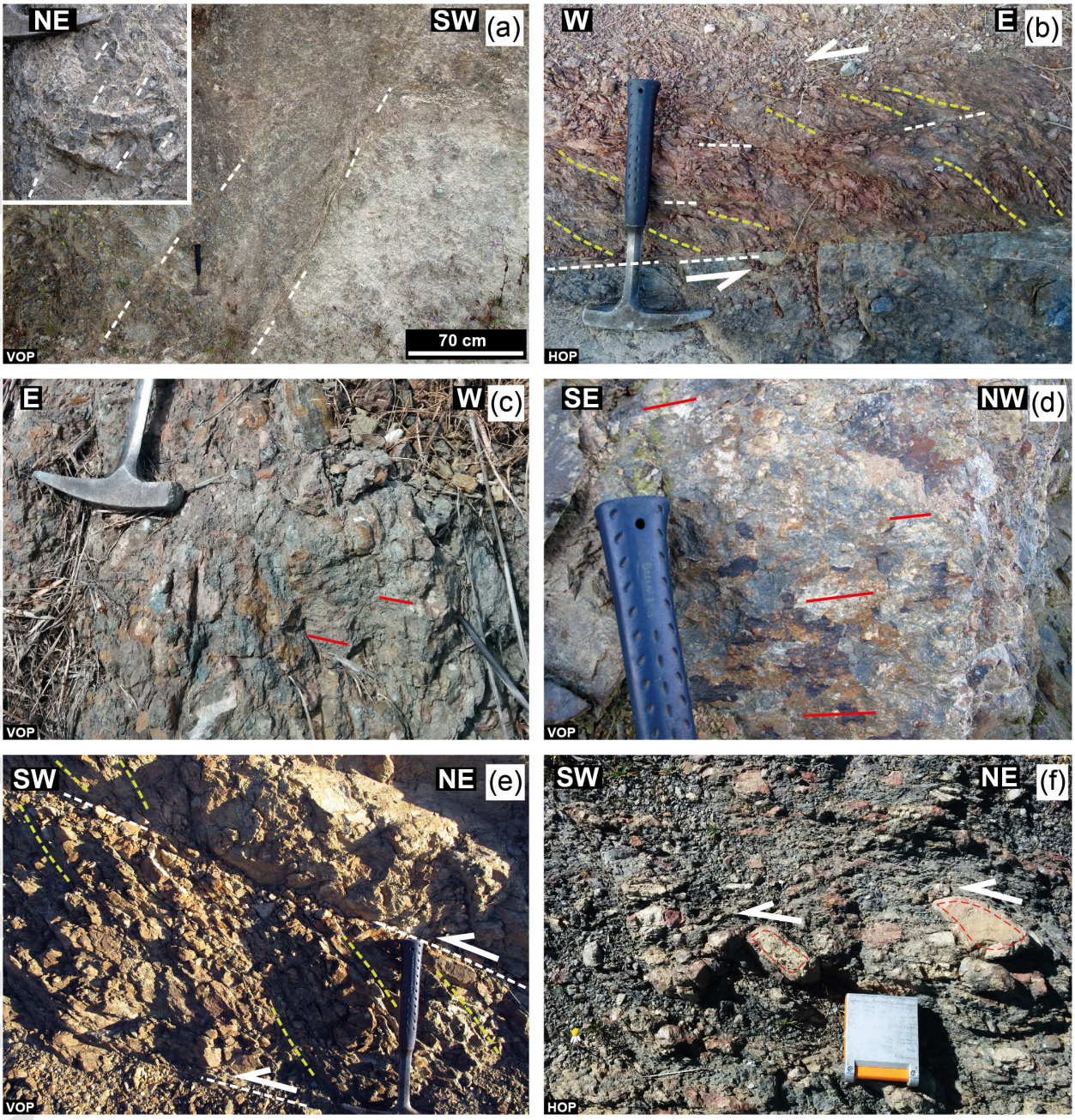

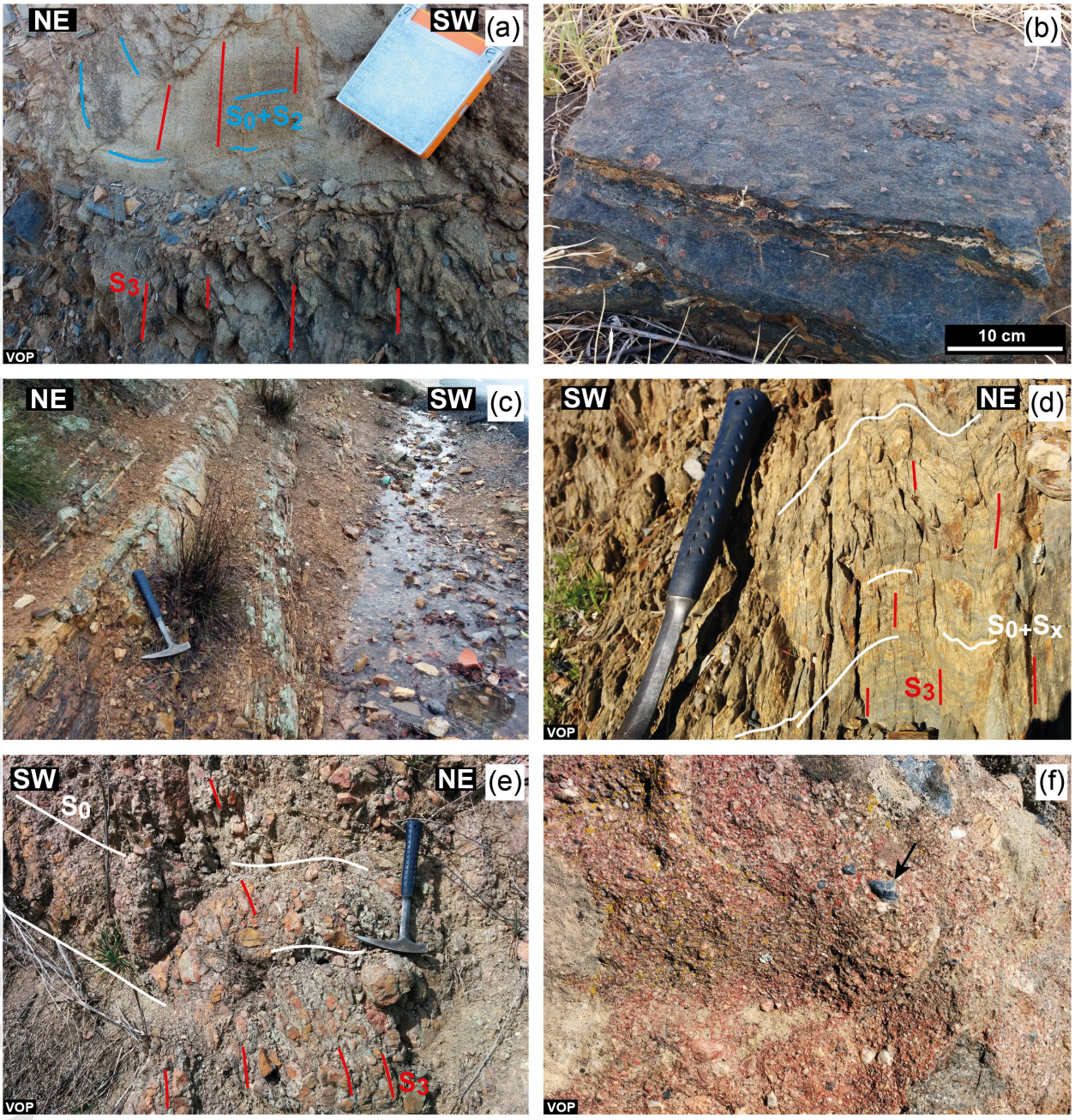

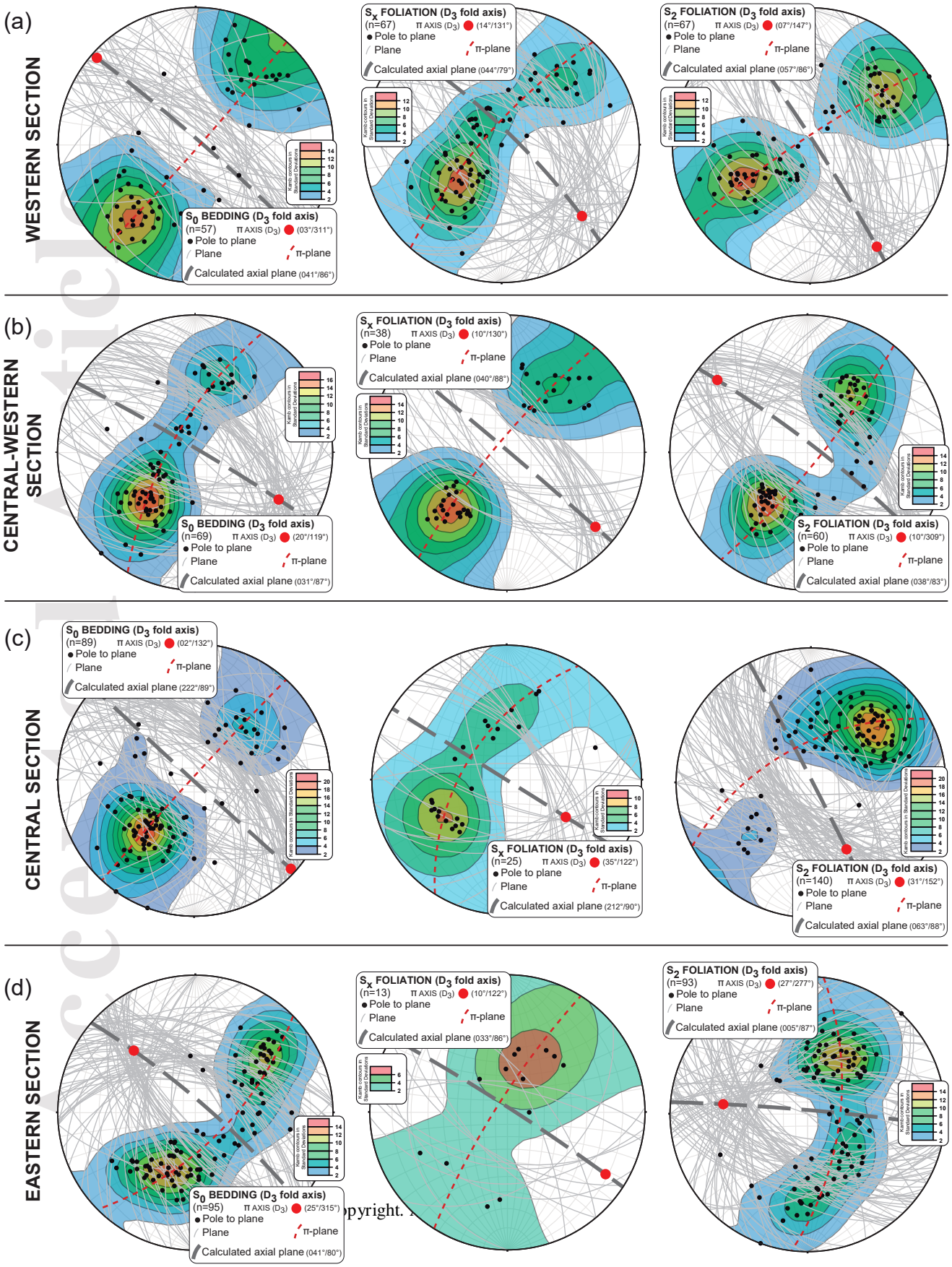
(a)
WESTERN SECTION
S0 BEDDING (D3 fold axis)
(n=57) π AXIS (D3) (03°/311°)
Pole to plane
Plane
π-plane
Calculated axial plane (041°/86°)
Sx FOLIATION (D3 fold axis)
(n=67) π AXIS (D3) (14°/131°)
Pole to plane
Plane
π-plane
Calculated axial plane (044°/79°)
S2 FOLIATION (D3 fold axis)
(n=67) π AXIS (D3) (07°/147°)
Pole to plane
Plane
π-plane
Calculated axial plane (057°/86°)
(b)
CENTRAL-WESTERN SECTION
S0 BEDDING (D3 fold axis)
(n=69) π AXIS (D3) (20°/119°)
Pole to plane
Plane
π-plane
Calculated axial plane (031°/87°)
Sx FOLIATION (D3 fold axis)
(n=38) π AXIS (D3) (10°/130°)
Pole to plane
Plane
π-plane
Calculated axial plane (040°/88°)
S2 FOLIATION (D3 fold axis)
(n=60) π AXIS (D3) (10°/309°)
Pole to plane
Plane
π-plane
Calculated axial plane (038°/83°)
(c)
CENTRAL SECTION
S0 BEDDING (D3 fold axis)
(n=89) π AXIS (D3) (02°/132°)
Pole to plane
Plane
π-plane
Calculated axial plane (222°/89°)
Sx FOLIATION (D3 fold axis)
(n=25) π AXIS (D3) (35°/122°)
Pole to plane
Plane
π-plane
Calculated axial plane (212°/90°)
S2 FOLIATION (D3 fold axis)
(n=140) π AXIS (D3) (31°/152°)
Pole to plane
Plane
π-plane
Calculated axial plane (063°/88°)
(d)
EASTERN SECTION
S0 BEDDING (D3 fold axis)
(n=95) π AXIS (D3) (25°/315°)
Pole to plane
Plane
π-plane
Calculated axial plane (041°/80°)
Sx FOLIATION (D3 fold axis)
(n=13) π AXIS (D3) (10°/122°)
Pole to plane
Plane
π-plane
Calculated axial plane (033°/86°)
S2 FOLIATION (D3 fold axis)
(n=93) π AXIS (D3) (27°/277°)
Pole to plane
Plane
π-plane
Calculated axial plane (005°/87°)

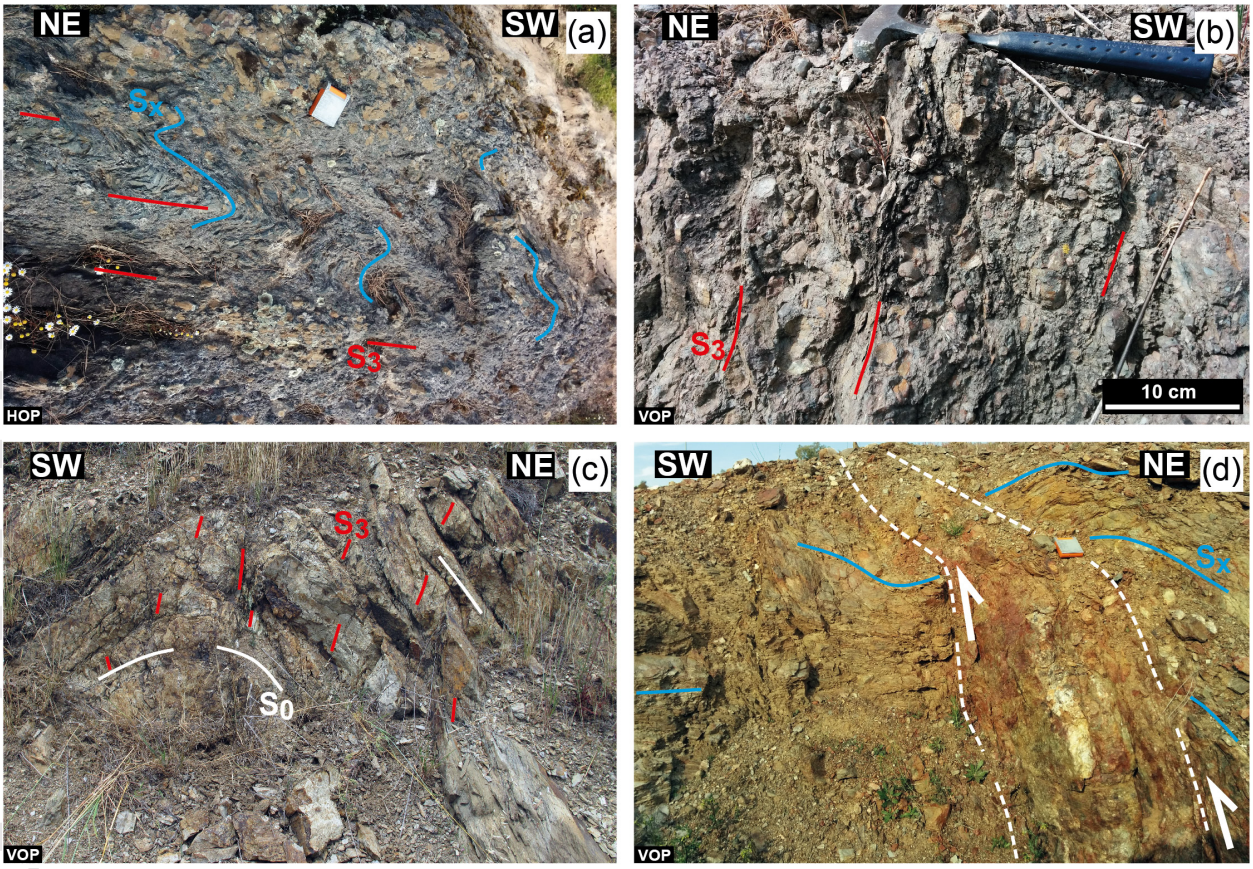

(a)

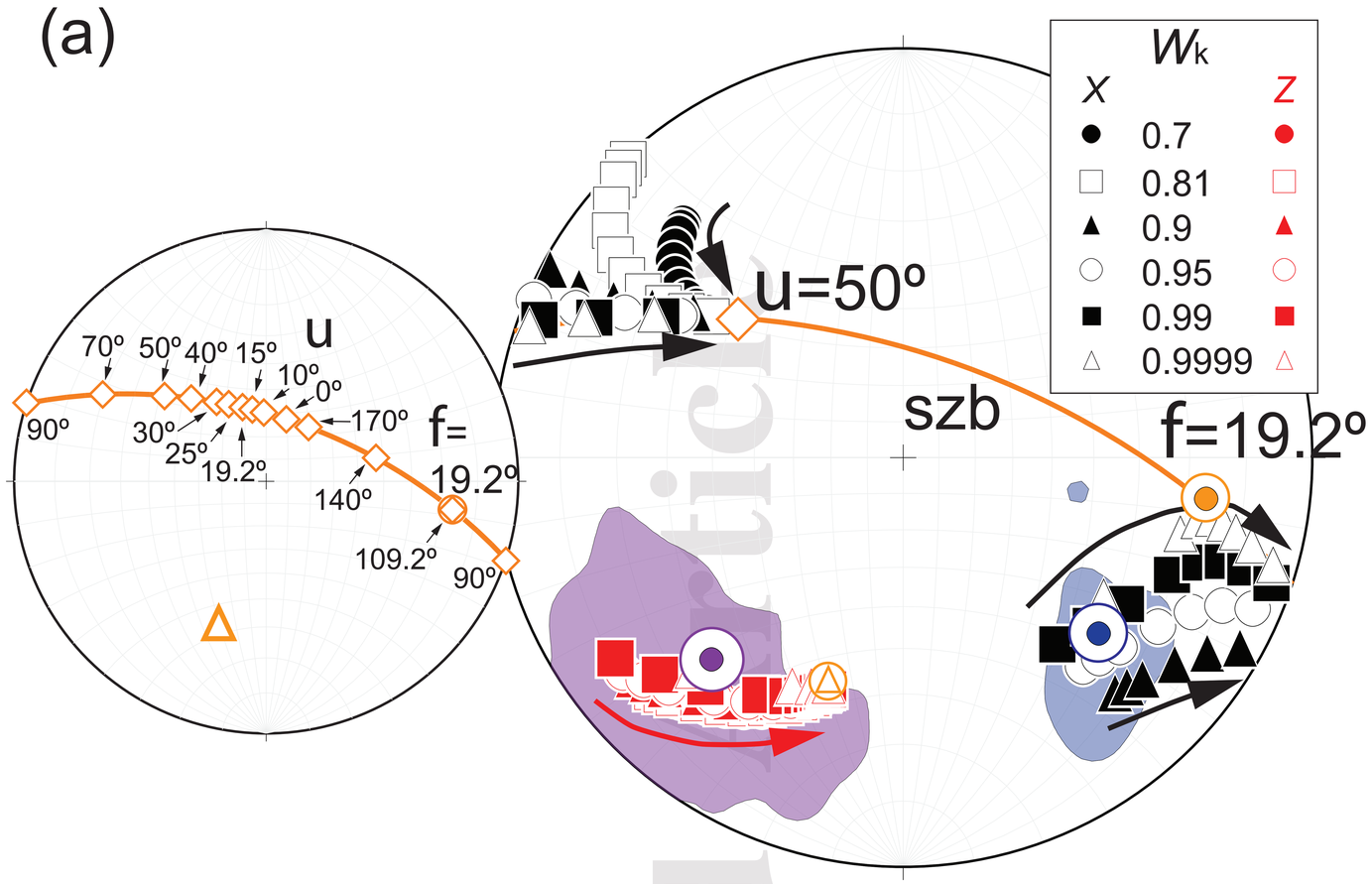

(b)

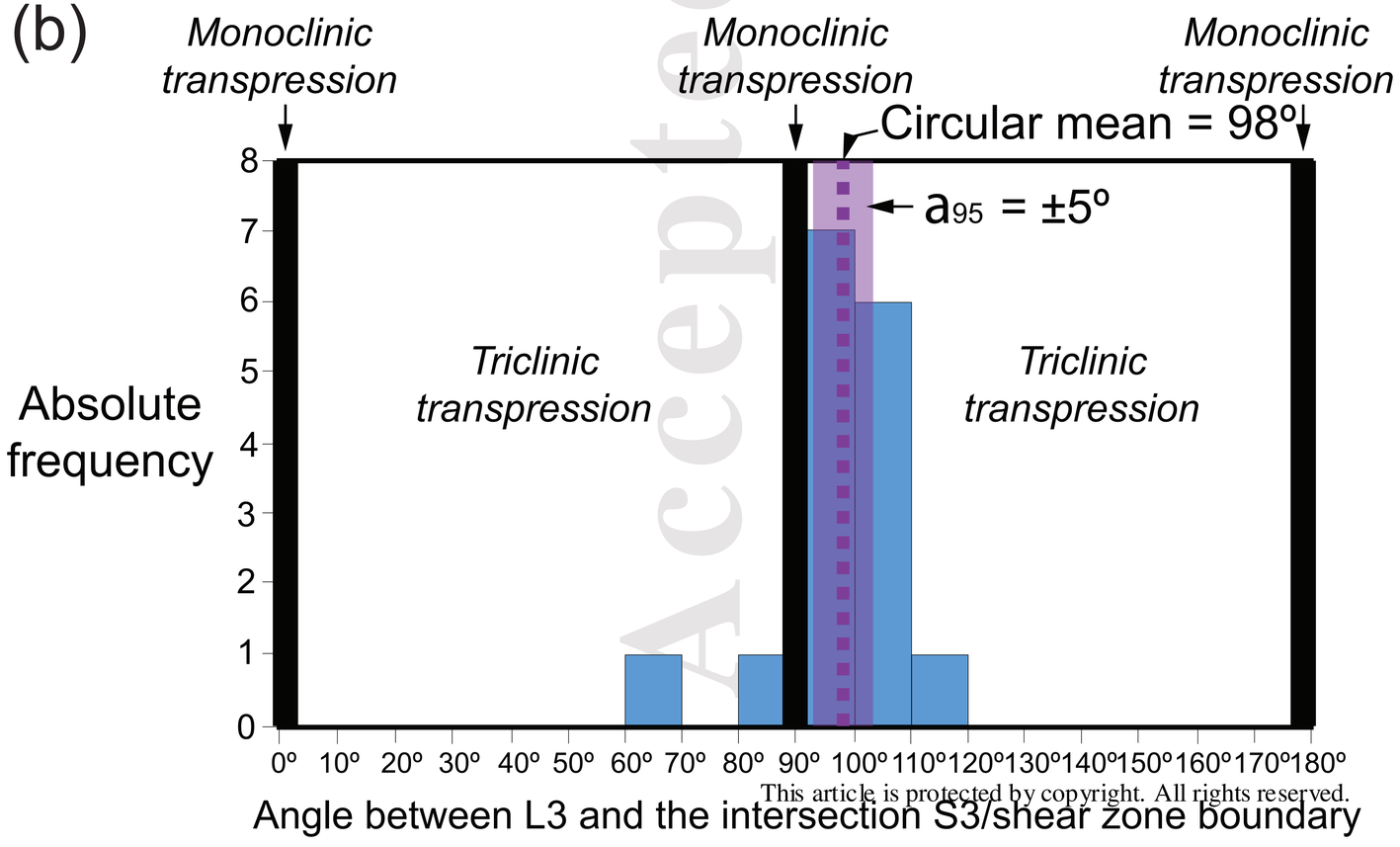

(c)

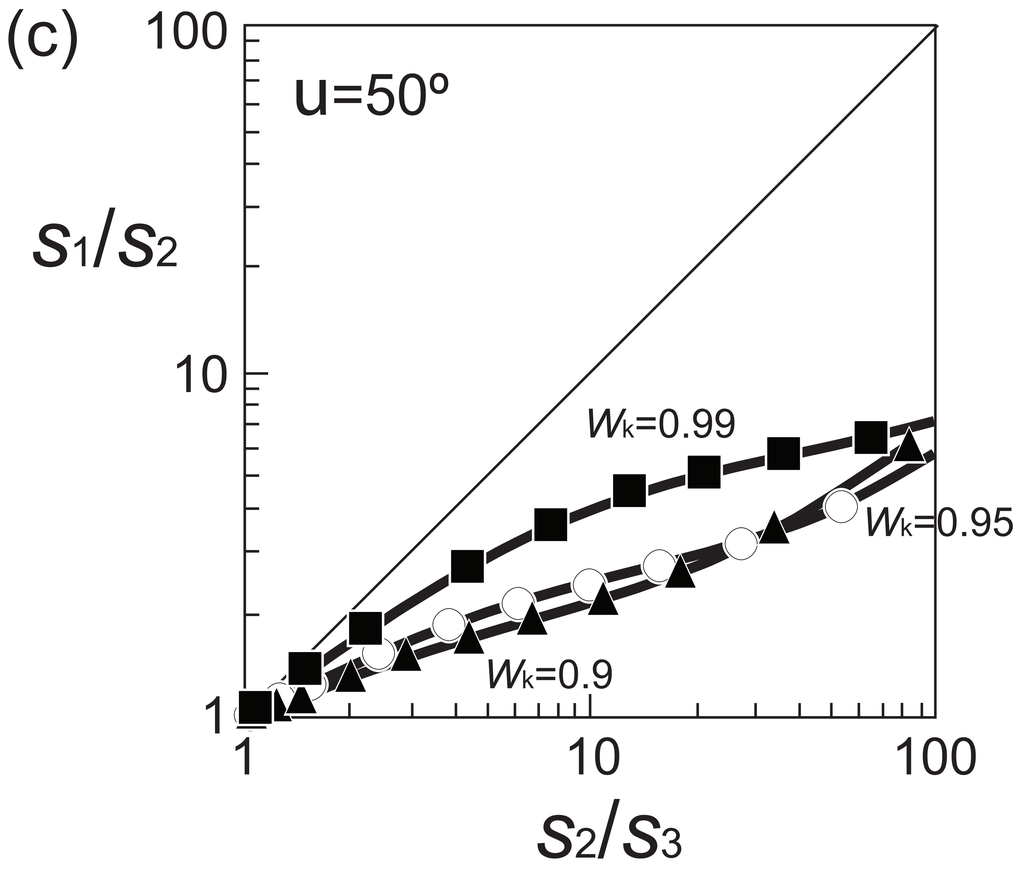

(d)

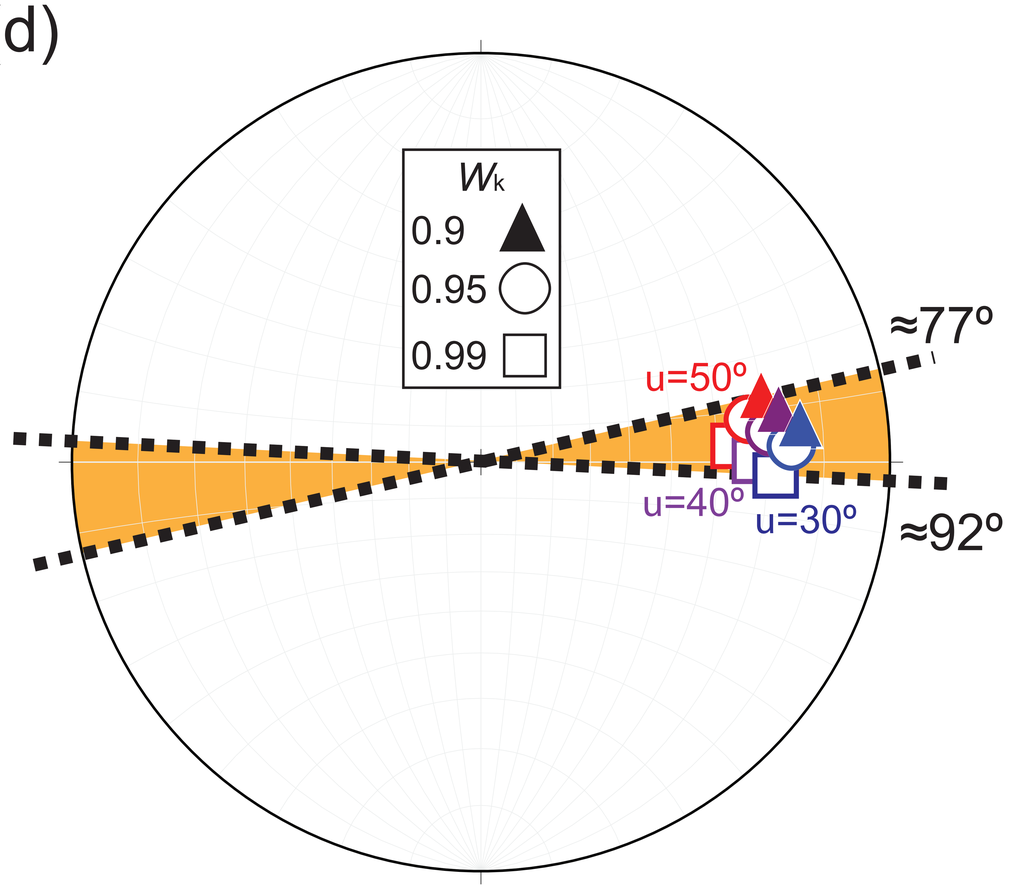

(a)

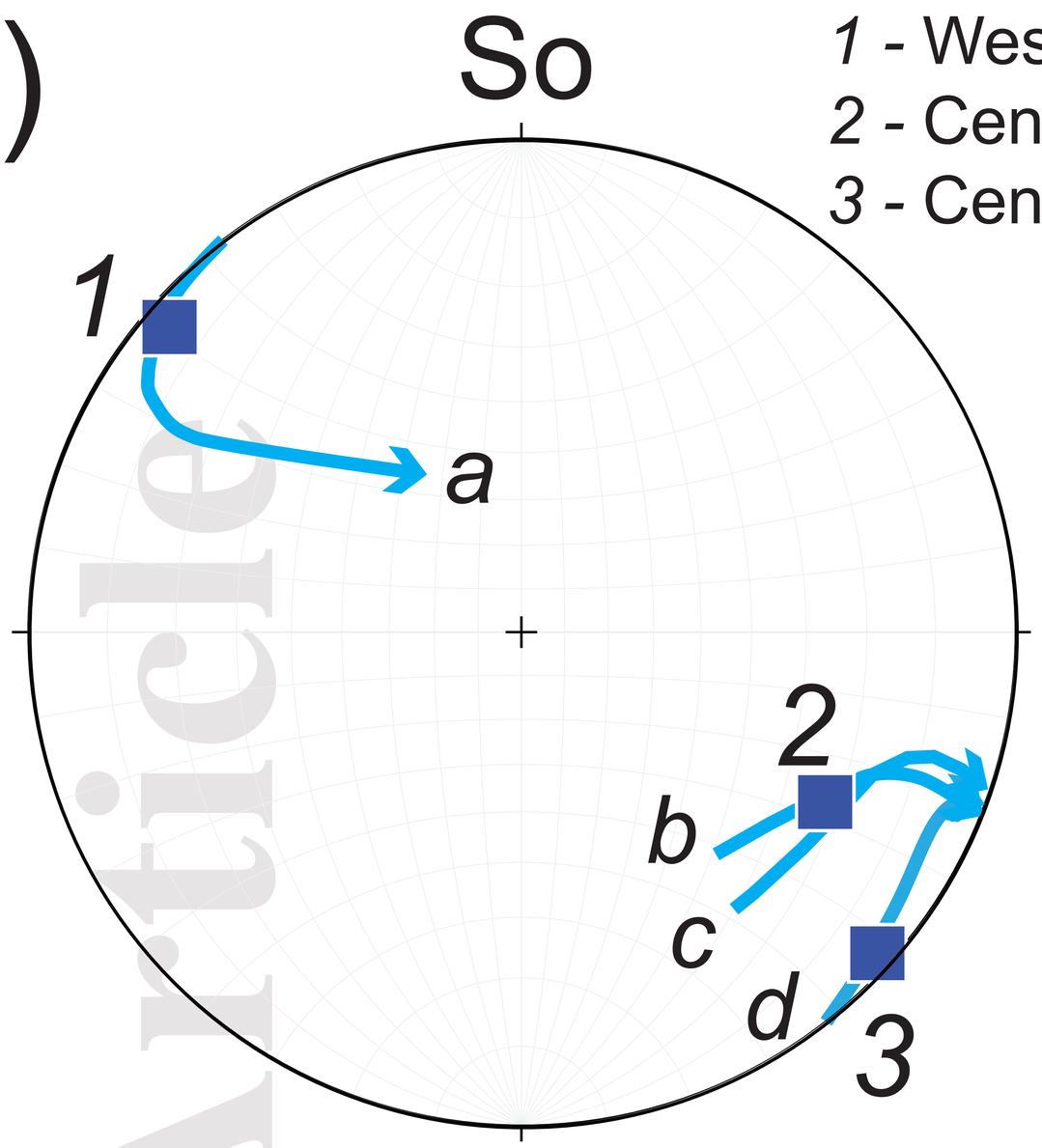

1 - Western section
2 - Central-western section
3 - Central section

(b)

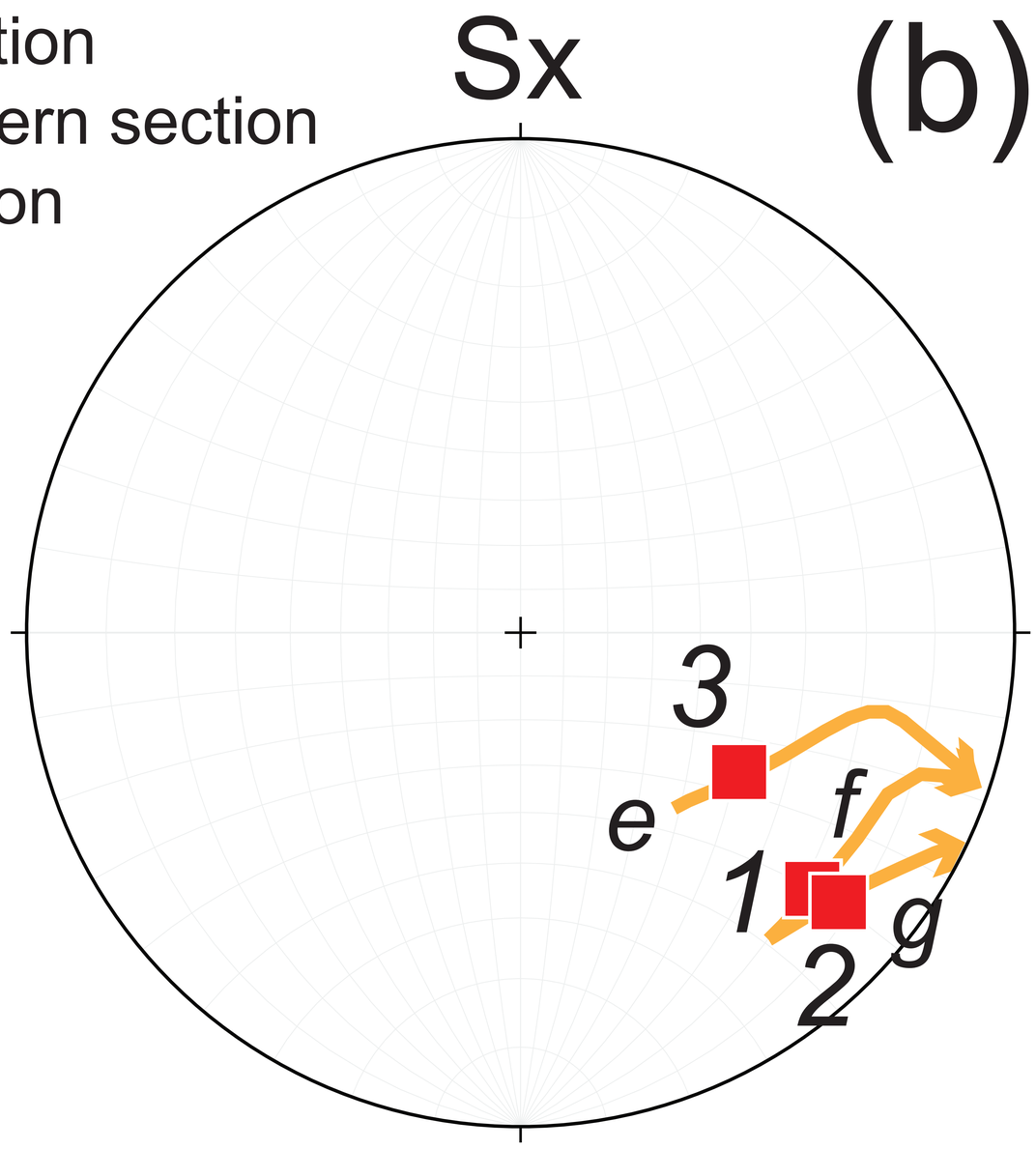

(c)

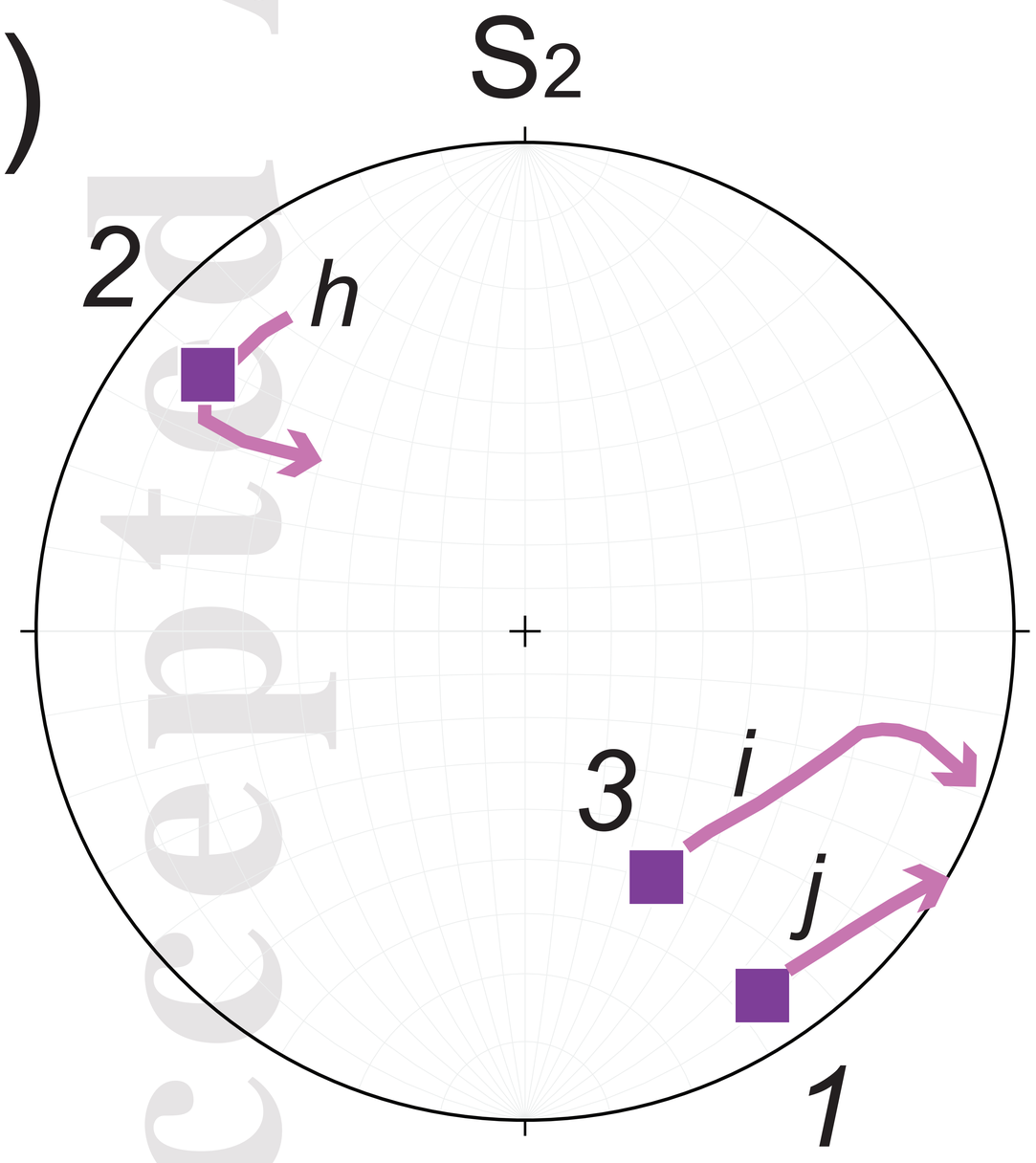

	Mean pole	a_{95}
So	83º→311º	11º
Sx	67º→336º	11º
S_2	80º→45º	14º

(d)

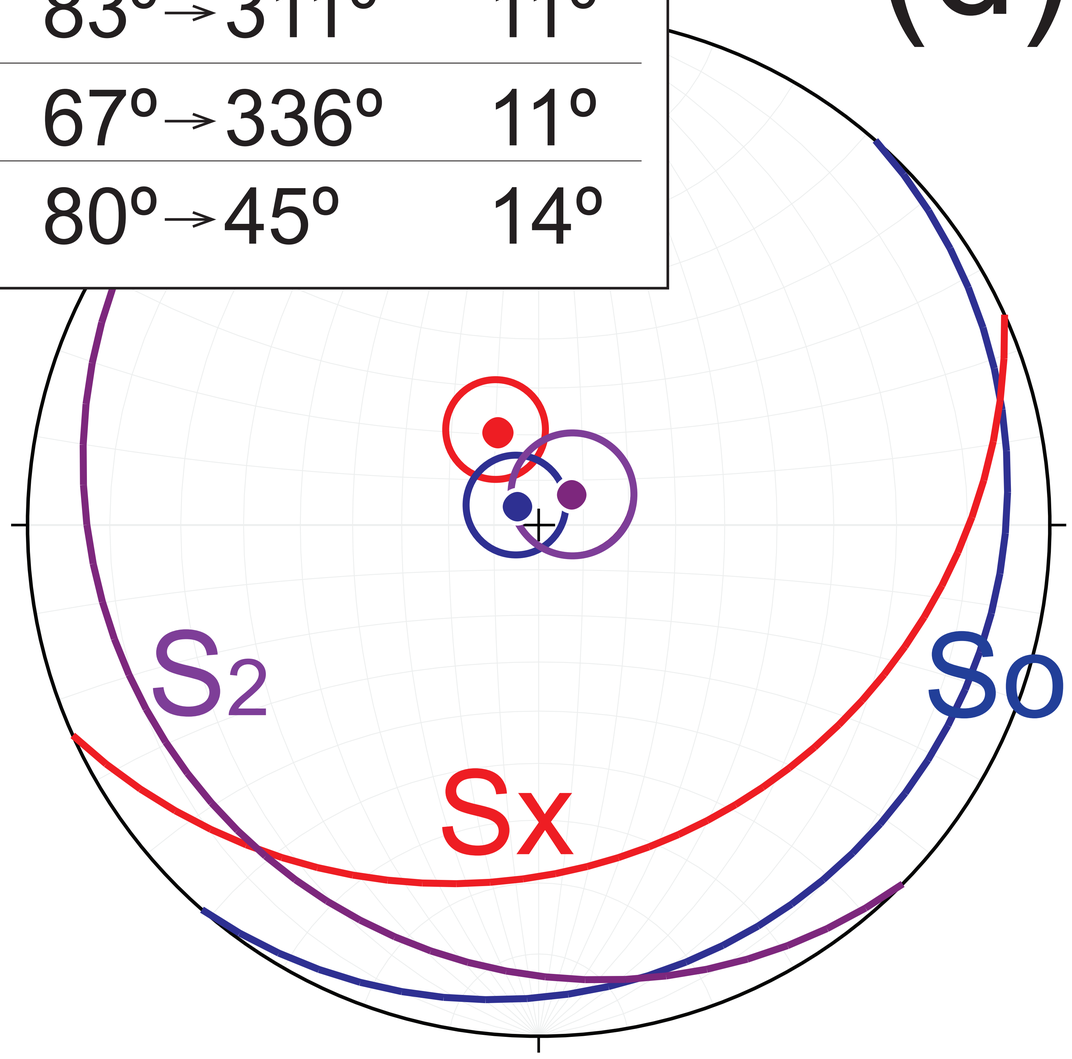

a: u=30º; W_k=0.9; N0ºE/0º

b: u=30º; W_k=0.9; N0ºE/40ºE

c: u=30º; W_k=0.99; N60ºE/20ºE

d: u=50º; W_k=0.9; N0ºE/0º

e: u=30º; W_k=0.99; N60ºE/40ºE

f: u=30º; W_k=0.99; N0ºE/20ºE

g: u=30º; W_k=0.9; N0ºE/20ºE

h: u=50º; W_k=0.9; N0ºE/20ºW

i: u=30º; W_k=0.99; N90ºE/40ºS

j: u=30º; W_k=0.9; N120ºE/20ºSW

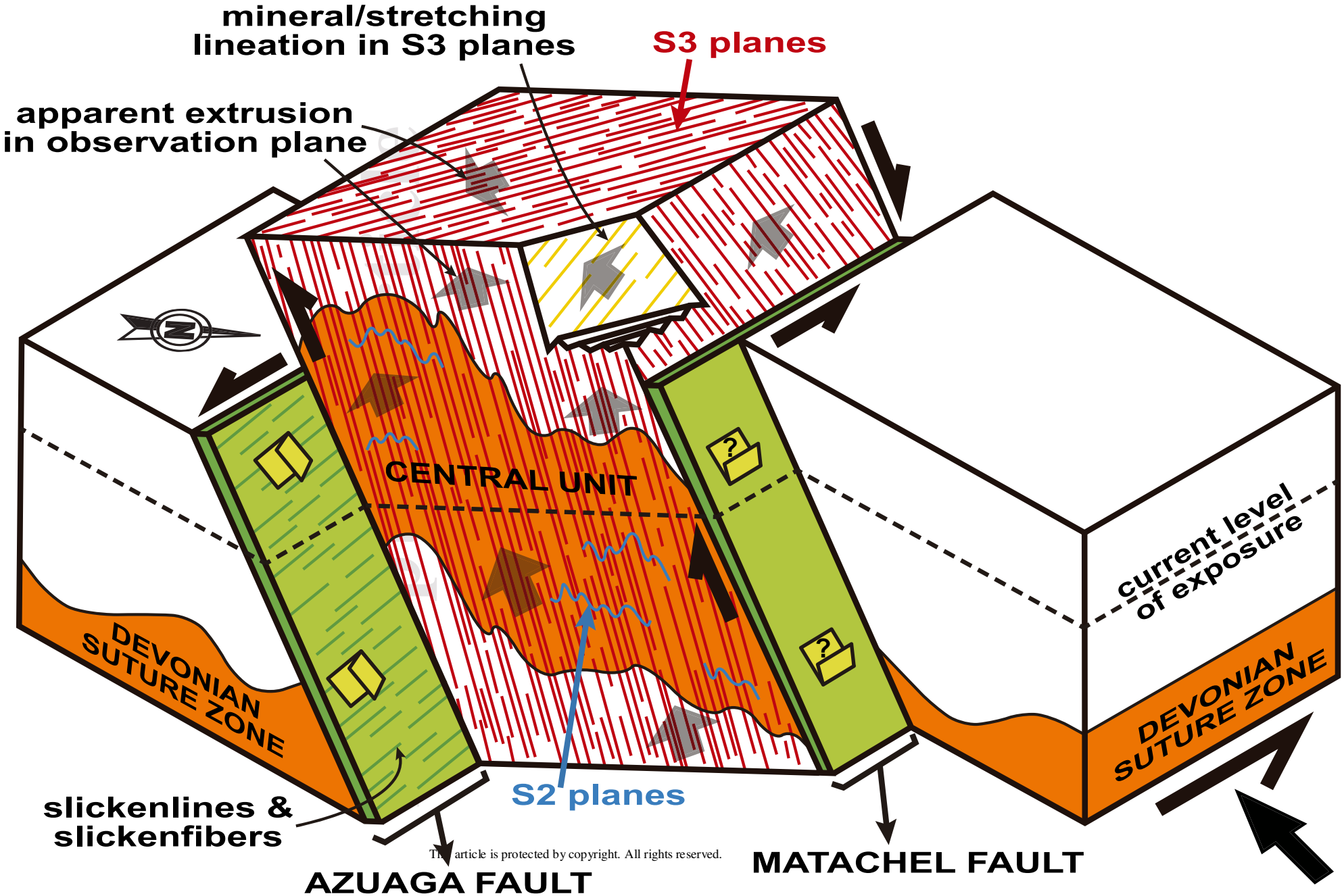

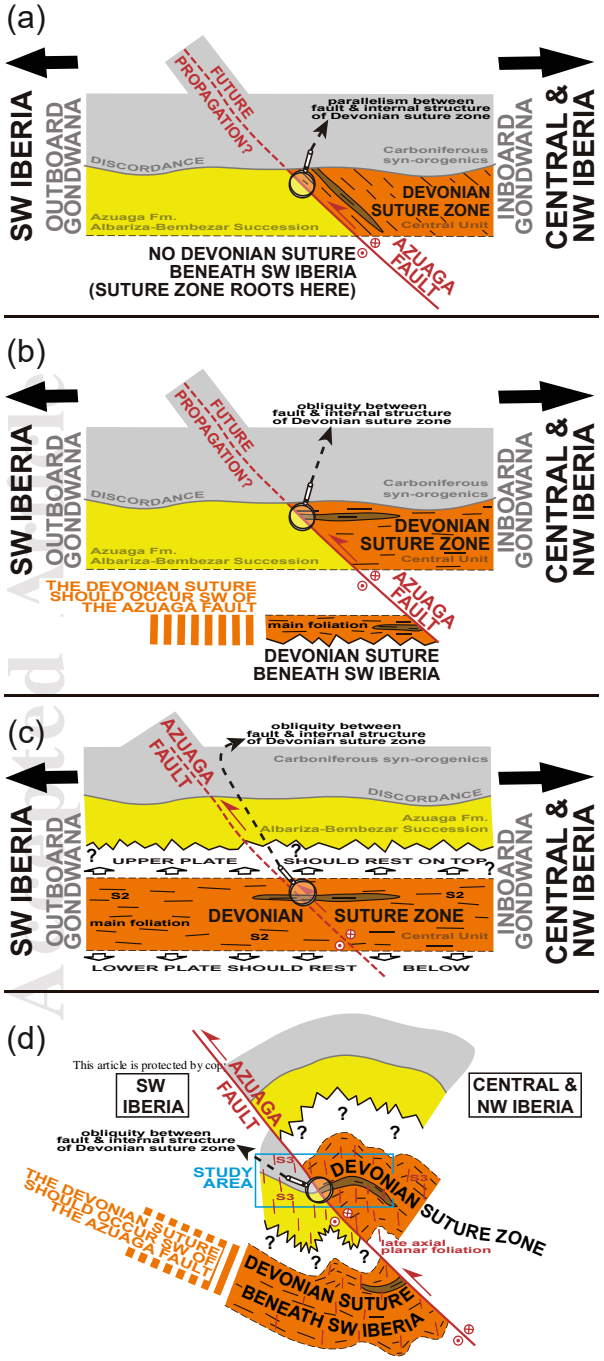
(a)
SW IBERIA
OUTBOARD GONDWANA
FUTURE PROPAGATION?
parallelism between fault & internal structure of Devonian suture zone
Carboniferous syn-orogenics
DISCORDANCE
DEVONIAN SUTURE ZONE
Central Unit
Azuaga Fm.
Albariza-Bembezar Succession
INBOARD GONDWANA
CENTRAL & NW IBERIA
AZUAGA FAULT
NO DEVONIAN SUTURE BENEATH SW IBERIA (SUTURE ZONE ROOTS HERE)
(b)
obliquity between fault & internal structure of Devonian suture zone
THE DEVONIAN SUTURE SHOULD OCCUR SW OF THE AZUAGA FAULT
main foliation
DEVONIAN SUTURE BENEATH SW IBERIA
(c)
UPPER PLATE SHOULD REST ON TOP
S2
DEVONIAN
LOWER PLATE SHOULD REST BELOW
(d)
This article is protected by cop
STUDY AREA
S3
late axial planar foliation